An assessment of bottom current controlled sedimentation in Pacific Ocean abyssal environments

C. Juan*, D. Van Rooij, W. De Bruycker

Department of Geology, Faculty of Sciences, Ghent University, Krijgslaan 281, S8, 9000 Gent, Belgium

ARTICLE INFO

ABSTRACT

The effect of the circulation of polar-sourced dense waters on the deep seafloor is still largely unknown. This paper presents multibeam bathymetric evidence for the existence of present-day contourite drifts on the central Pacific ocean at depths ranging between 4000 and 5000 m, based on the identification of their diagnostic erosive (moats, linear moats, furrows and abyssal sinuous channels) and depositional (plastered, elongated separated and abyssal contourite-fan drifts) contourite morphological features. These contourite drifts display a patchy distribution, sculpted by the secondary flows of the Lower Circumpolar Water (LCPW) and the North Pacific Deep Waters (NPDW), as well as local dynamics of the flow in the form of internal waves and bottom currents modulated by tides, which are capable of accelerating the typically sluggish bottom currents and contribute to the erosion, transport and deposition of sediments. The formation of contourites is also predominantly controlled by the presence of large-scale tectonic and volcanic features (ridges, seamounts and deep elongated valleys), which affect the morphology and distribution of the basins and induce the acceleration of bottom currents. Overall, this study allows to re-assess the effects, distribution and significance of bottom-current controlled sedimentation in abyssal environments, where examples of contourite features are still rather scarce in part because of the technical challenges and their remote location, but also because the effect of bottom currents is not well known in the central oceanic basins and only capable of marginally affecting their sedimentological record.

1. Introduction

The role played by bottom currents on the sedimentary processes has been subject of the interest of the scientific community during the last decades (Stow et al., 2002a; Viana and Rebesco, 2007; Rebesco and Camerlenghi, 2008; Hernández-Molina et al., 2010; Van Rooij et al., 2016). The accessibility of the continental margins, their minor depths, the larger deposits generated by the input of terrigenous sediment (Faugères and Stow, 2008) as well as the action of large-scale currents have favoured obtaining abundant high-quality datasets in many disciplines (oceanography, sedimentology, geophysics…) (Howe, 2008) that have allowed a better understanding on how bottom-currents sculpt the margins and interact with other processes such as turbidite flows (Michels et al., 2002; Rebesco et al., 2007; Mulder et al., 2008). On the opposite, the role played by bottom currents in the deep abyssal part of the oceans has received far less attention (Hernández-Molina et al., 2008a), in part because the current regime was considered as non-favourable and mostly characterized by sluggish to very weak currents (Hollister, 1993; Zenk, 2001), and because observations are

particularly difficult to make due to the great distance from the coast and the large depths. As a result, high-quality datasets are scarce compared to continental slopes.

Bottom-current deposits were first recognized in the 1960s (Heezen and Hollister, 1964; Heezen et al., 1966) as deposits associated with the deep thermohaline circulation. The ever-growing number of deposits recognized as a product of the action of bottom currents as well as the identification of other oceanographic processes capable of reworking the seafloor (Shanmugam, 2008, 2014; Hernández-Molina et al., 2016) led to the reformulation of the original definition, naming "contourite features" those sediments deposited or substantially reworked by the persistent action of bottom currents (Stow et al., 2002b; Rebesco et al., 2014). Due to their higher sedimentation rates, contourites are ideal recorders for past climatological and oceanographic conditions (Stow et al., 2002b; Hernández-Molina et al., 2004; Llave et al., 2007; Faugères and Stow, 2008; Shanmugam, 2008). Besides, only the last decade the contourite paradigm is really advancing, with a better understanding between sedimentology and oceanographic processes (Stow et al., 2009).

---

* Corresponding author.
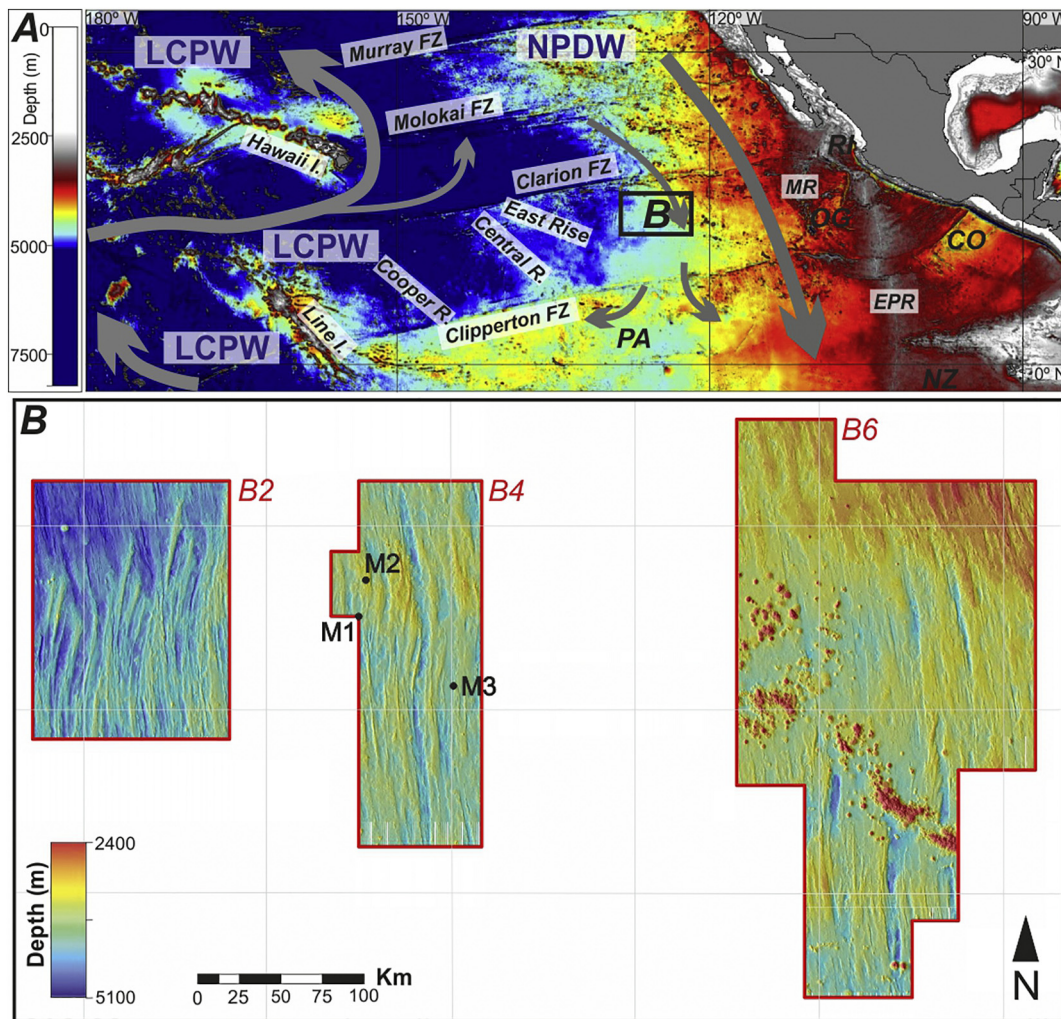 *E-mail address:* carmen.juanvalenzuela@ugent.be (C. Juan).

Fig. 1. A) Location and general bathymetric map of the Clarion-Clipperton Zone (CCZ) (source: GEBCO), including its most relevant geological features as well as the pathway of the deep-water currents (dark grey, based on Johnson and Toole (1993) and Rintoul (2013)). The thickness of the arrows indicating the current pathway offers an approximation to the distribution of major and minor branches of the bottom flow, but it is not proportional to their actual intensity. B) Bathymetric map of the study area (see location in inset A), with the three main boxes B2, B4 and B6 areas (data courtesy by Global Sea Mineral Resources NV), including the location of mooring data (Table 1). Legend: MR - Mathematicians Ridge, EPR - East Pacific Rise, PA – Pacific Plate, RI – Rivera Plate, CO – Cocos Plate, NZ – Nazca Plate, OG – O'Gorman plate, LCPW – Lower Circumpolar Water, NPDW – North Pacific Deep Water.

The tropical Pacific Ocean is a prime target for paleoceanographic studies due to its important role on Earth's climate, being one of the main heat collectors feeding the thermohaline circulation (it represents more than half of the tropical oceans) and modulating CO_2 exchanges with the atmosphere (Dubois and Mitchell, 2012). Within the tropical Pacific, the seafloor of the Clarion-Clipperton Zone (CCZ) (Fig. 1a) is an area where contourites may be potentially identified, due to the well-known presence of ferromanganese nodules which require bottom currents for their genesis and growth (Pautot and Melguen, 1975; Margolis and Burns, 1976; Pautot and Melguen, 1979; Glasby et al., 1982; von Stackelberg and Beiersdorf, 1991). In turn, testing the presence of bottom currents and other deep-water processes such as internal waves, tides, benthic storms, eddies and vortices, which are considered capable of generating depositional and erosional features in abyssal plains (Gao et al., 1998; He et al., 2008; Hernández-Molina et al., 2008b) may also allow to better specify and predict the occurrence of ferromanganese nodules, and provide more successful coring sites for palaeoclimatological sampling. Although many examples of deep-water contourites (below 2000 m deep) are known to the scientific community, most of them are located near on continental margin with fewer being located at abyssal plains, in the "centre" of the ocean, in part because sediment supply is trapped on the margins, in the trenches

and marginal seas (Hernández-Molina et al., 2008a). Scarce examples have been identified so far in the central Pacific ocean (Johnson and Johnson, 1970; Johnson, 1972; Lonsdale, 1981; Shipley et al., 1985; Beiersdorf, 1987; von Stackelberg and Beiersdorf, 1991; Dubois and Mitchell, 2012) despite it has been subject of intense research during the last decades for nodule exploration (Price and Calvert, 1970; Margolis and Burns, 1976; Craig, 1979; Hoffert, 1980; Glasby et al., 1982; Hein et al., 1997; Han et al., 2003; Hoffert, 2008; Kim et al., 2012; Mewes et al., 2014).

In the Pacific Ocean the sedimentary cover on the basaltic substrate is generally known to be controlled by the age of the crust, the regional and local tectonic history, the presence of structural trends in the basement, the distance to the sediment source and the sedimentary processes transporting the sediments (Divins, 2003). The presence of obstacles has also direct consequences on the sedimentary processes by deflecting the bottom currents that sweep the seafloor (Roden, 1987), and locally favouring downslope processes. The sedimentary cover in the tropical Pacific has been described to result from two different idealized models of sedimentation: *sediment drape* and *basin fill* (Dubois and Mitchell, 2012). Basin fill dominates in the early stages of the basin evolution, when the sediment is either preferentially deposited or re-worked by bottom currents into depressions, which act as sediment

traps (Shipley et al., 1985). After the partial infilling of the seafloor irregularities, sediment draping throughout a region was seen to be dominant, caused by the even settling of sediment through the water column (Shipley et al., 1985; Dubois and Mitchell, 2012). These two idealized models are just extremes in a continuum, and both can act simultaneously in a more complex and realistic sedimentation pattern (Dubois and Mitchell, 2012) where the sediment fluctuates greatly over short distances (Mitchell et al., 2003) and has been estimated to be 20–30% thicker within morphological depressions than on the abyssal hills (Shipley et al., 1985). It is however relevant to stress that only one of the idealized models (basin infill) considers the action of bottom currents as a relevant factor in the sedimentation pattern, favouring sediment focusing (dissolution and lateral redistribution of the sediment before its sedimentation) (Marcantonio et al., 2001; Mitchell et al., 2003; Dubois and Mitchell, 2012), as well as winnowing and erosion of sediment already deposited off local highs due to the action bottom currents (Shor, 1958; Shipley et al., 1985; Mitchell et al., 2003).

In order to better understand how the various obstacles affect the local morphology and the generation of sedimentary basins as well as how (and where) contourite drifts are distributed in the deep Pacific Ocean, new high-resolution multibeam bathymetry data recorded by the Belgian company Global Sea Mineral Resources NV in a portion of the seafloor located in the eastern CCZ (between 12–17˚N and 129–122˚W) will be analyzed (Fig. 1b).

The objectives of this present study include: (i) to examine the role on morphology of the past and present geodynamic framework, (ii) to analyze how the various geomorphological features affect the generation, characteristics and distribution of the sedimentary basins, (iii) to examine the current-related features identified inside, and (iv) together with the current knowledge on the regional abyssal flow regime, to interpret the role played by the different water masses and flow regimes in their genesis and to deduct where it is more likely to find current-related deposits. The main aim of this study is to provide a first morphological characterization of abyssal contourite drifts, and to better understand their distribution and spatial significance.

2. Regional setting

2.1. Geological setting

The age of the basaltic oceanic crust within the CCZ ranges between Cretaceous and Miocene (Müller et al., 2008; Barckhausen et al., 2013), and its sediment cover varies in thickness from about 400 m near the Line Islands (west), to 25 m of sediments near the Mathematicians Ridge (east) (Whittaker et al., 2013). The CCZ morphology broadly consists of ridges and depressions generated by parallel faulting on the flanks of the East Pacific Rise (EPR) (Macdonald et al., 1996). Further fracturing of the basaltic substrate was caused by the cooling and contraction of the oceanic lithosphere as it was displaced away from the EPR (Yubko, 2016), forming elongated abyssal hills of N-S to NNW-SSE orientation (Menard, 1964), typically 10–30 km long, 2–5 km wide and approximately 50–300 m high (Macdonald, 1998; Rühlemann et al., 2011; Mewes et al., 2014). These abyssal hills are interspersed by seamounts (> 1000 m), knolls (200–1000 m) and highs (< 200 m) (Schmidt and Schmincke, 2000; Fisher and Wheat, 2010; Staudigel and Clague, 2010) that typically result from off-axis volcanic activity, as well as some seamount chains (Rühlemann et al., 2011) generated through intra-plate volcanism (Batiza, 1982; Smith and Jordan, 1988; Wessel et al., 2010). Less frequent obstacles found in the CCZ seafloor fabric include large-scale ridges (East, Central and Cooper Rises, Fig. 1a) (Kotlinski et al., 2009) and faults (Macdonald et al., 1996; Macdonald, 1998; Yubko, 2016). This initial seafloor morphology was further influenced and modified by several tectonic events (Herron, 1972; Menard, 1978; Smith, 2007; Yubko, 2016) as well as significant changes in the plate motions that were reflected in seafloor spreading anomalies and bends in the fracture zones (Barckhausen et al., 2013),

including the rotation of the EPR (Klitgord and Mammerickx, 1982) and the abandonment of several ridge fragments.

During a brief period (until 6.5 Ma), a double accretion system was active west of the Cocos plate, and after a jump of the spreading axis associated to intense re-fracturing and faulting the Mathematicians ridge was finally abandoned (Anderson and Davis, 1973).

Within the study area, the age of the basement has been estimated to be of Oligocene age based on magnetic anomaly data (Müller et al., 2008), varying from 24.5 Ma in the east, up to 30.5 Ma in the west. The expected sediment thickness varies from 50 m in the east to ~100 m in the west (Divins, 2003; Whittaker et al., 2013).

2.2. Oceanographic setting

The water masses present in the Eastern Tropical Pacific Ocean can be roughly divided into upper (< 400 m), intermediate (500–1000 m) and deep (> 1500 m) water masses, separated by the mixing zones between the different water masses. Among them, the water masses that sweep the seafloor and dominate the deep Pacific are the Lower Circumpolar Water (LCPW) and the North Pacific Deep Water (NPDW) (Fig. 1a) (Johnson and Toole, 1993; Wijffels et al., 1996). The LCPW is defined by cold and dense waters of Antarctic origin with high salinity and oxygen concentrations (Johnson, 1972; Wijffels et al., 1996; Mewes et al., 2014) and low dissolved silica content, which result from the mixture of North Atlantic Deep Water (NADW), Antarctic Intermediate Water (AAIW) and older LCPW (Johnson and Toole, 1993). On the other hand, the NPDW is the end-product of the slow warming and freshening of LCPW, with low oxygen and high dissolved silica concentrations acquired from in situ dissolution in the water column as well as long contact with sediments (Talley and Joyce, 1992; Johnson and Toole, 1993; Wijffels et al., 1996). LCPW is colder and denser than NPDW, causing part of the latter to flow over a wedge of oxygen-rich LCPW (Mitchell et al., 2003). In addition, the longitudinal transition from one water mass to another may suffer seasonal and inter-annual variations (Macdonald et al., 2009) depending on climatic fluctuations.

The deep flow pattern shows a main stream of LCPW on the western boundary of the Pacific Basin, splitting in several branches and with an eastward branch in the northern equatorial area (Mantyla and Reid, 1983; Tsuchiya and Talley, 1996) (Fig. 1a). Water mass conversion from LCPW to NPDW takes place in the North Pacific, and the previously described northward flow is balanced by a southward flow of NPDW, which moves in a strong southward flow over the western flank of the East Pacific Rise in the Northeast Pacific Basin (Fig. 1a) that becomes a very sluggish flow in the Central Pacific Basin (Johnson and Toole, 1993), turning westward near 10˚S, and southeastward near 130˚W (Reid, 1986) (Fig. 1a). Last, according to the model built by Macdonald et al. (2009), the southwards transport of NPDW exits the Pacific Basin east of 110˚W, flowing just west of South America.

Bottom currents in the CCZ have been already documented by several studies (Amos et al., 1977; Hayes, 1979; Hayes, 1980; Demidova and Kontar, 1989; Demidova et al., 1993, 1996; Kotlinski et al., 1996; Morgan et al., 1999), as well as other phenomena such as internal waves and tides (Hayes, 1979; Hayes, 1980; Shanmugam, 2013) and benthic storms (Hollister and McCave, 1984; Demidova et al., 1993, 1996). Based on current meter data, three different modes of current intensity have been identified in the CCZ (Demidova et al., 1996; Morgan et al., 1999): calm periods with minimal current speed (0–3 cm/s) and headed slightly NW, intermediate tidal periods with variable current speed (0–6 cm/s) and direction (NW and SE), and occasional benthic storms reaching up to 15 cm/s in 1 h average and headed SE.

Within the study area, peak velocities as high as 25 cm/s (Amos et al., 1977; Mewes et al., 2014) were detected (Table 1). The average flow direction in the mooring with largest duration was headed northwestward, with periodical shifts to a southward flow during several weeks and velocities ranging between 1 and 9 cm/s with peaks of

Table 1
Current meter data described in the literature located within the study area (see Fig. 1b for location).

Mooring ID	Location	Distance above seafloor (m)	Depth (m)	Time of the mooring	Duration (d)	Average flow direction	Velocity data	Max speed (cm/s)	Reference
M1	15°N, 126°W	10	4606	April–May 1975	34	SW	Semidiurnal peaks.	25	Amos et al., 1977
M2	15°13′N, 125°58′W	10	4655	–	11	W	Average speed of 7 cm/s.	–	Morgan et al., 1999
M3	14°38′N, 125°29′W	6 and 30	4508	4th July to 8th December 1977	156	NW, with periodical shifts to a S flow.	Non-stationary internal wave motions.	13 and 15	Hayes, 1979; Hayes, 1980

13–15 cm/s (Hayes, 1979; Hayes, 1980; Mewes et al., 2014) (Table 1, M3). These registers confirm the complex oceanographic regime, which is tidally influenced (Amos and Roels, 1977; Amos et al., 1977; Demidova et al., 1996; Morgan et al., 1999) under the control of latitudinal and seasonal variations (Shanmugam, 2013), and locally variable. These current metres also suggest the influence of both water masses in the study area, affected by the northwards-directed LCPW and with periods of southward NPDW flow (Table 1, M3) associated to changes in the temperature (Hayes, 1980).

3. Material & methods

The study areas are located between 12–17°N and 129–122°W and are named B2 (17,869 km²), B4 (which combined with the overlapping Deep Ocean Mining Environmental Study DOMES-C area reaches 16,472 km²) (Bischoff and Piper, 1979) and B6 (44,005 km²), from west to east (Fig. 1b). The three areas include various seafloor contexts that will contribute to obtain a better understanding between its sedimentary regime and oceanographic processes.

The dataset (Fig. 1b) was provided by the Belgian company Global Sea Mineral Resources NV, and was obtained during a survey carried out in 2014 on board of the RV Mt. Mitchell (Global Seas). The vessel was equipped with a hull-mounted Kongsberg EM120 Multibeam Echosounder (2 × 2°, 12 kHz), with 191 yaw, pitch and roll stabilized beams, which allowed to obtain a 75 m per pixel map of the bathymetry and the backscatter response of the seafloor. The positioning and altitude data were provided in real time using an Applanix POS MV 320 motion platform, operating on two GPS receivers. To correct the dataset, the sound velocity was measured two times per day at intervals of 12 h with Sippican T-5 XBT's. The data processing (including correction of the velocity of the sea water and removal of noise in the dataset) was conducted using Caris HIPS & SIPS 8.1 software.

The identification of the main sedimentary basins, large-scale topographic obstacles and possible locations favourable to contourite deposits, as well as discerning on a smaller scale the various sedimentary features sculpted within the basins and around the positive structures has required detailed analyses using various cartographic tools and geographic information systems. Most analysis of the data and mapping was performed both with ArcGIS Desktop 10.4.1 and Global Mapper 16. The process of identifying the sedimentary basins consists of four main steps (Fig. 2):

With the purpose of comparing the features present on a basement with westward increasing depth, A) the bathymetry was averaged with a focal filter with the same order of magnitude as the width in cross-section of the most prominent feature (Fig. 2). B) This smoothened and averaged bathymetry was subtracted from the original bathymetry (Fig. 2), so all the basins, ridges, seamounts, etc. are displayed according to their relative context within a 15 km radius because bathymetric data tend to be spatially autocorrelated (Weiss, 2001). C) With the purpose of enhancing the sedimentary basins within their relative context, various filters were calculated. All the areas with positive mean elevations (> 0 m) were blanked with a buffer of 25 m set as partly transparent (Fig. 2). Additionally, all the areas with a slope in excess of 15° were also blanked, based on the assumption that those must

correspond to features with tectonic or volcanic origin (i.e., fault lineations, exposed flanks of abyssal hills) (Fig. 2). D) Last, in order to highlight the small-scale depressions and mounded features within the basins and valleys, a fine scale Bathymetric Position Index (BPI) (Weiss, 2001; Verfaillie et al., 2007; Wright et al., 2012) was calculated (Fig. 2), resulting in a negative value for depressions and concave features (such as the base of a slope) and positive values for elevations and upper slope breaks.

The original bathymetry, the seafloor backscatter, as well as the filtered BPI which results of this workflow (highlighted in red in Fig. 2) will be compared to optimize the identification of the various small-scale features. The identification of the seamounts, knolls and highs was carried out using an automated procedure based on recently developed Python scripts for ArcGIS (Gafeira et al., 2015; De Clippele et al., 2017). Last, the identification of the contourite features was based on the criteria originally proposed by Faugères et al. (1999) and later improved and updated with the input of many authors (Stow et al., 2002a; Viana and Rebesco, 2007; Rebesco and Camerlenghi, 2008; Rebesco et al., 2014; Van Rooij et al., 2016). The terminology of Faugères et al. (1999) and Rebesco et al. (2014) was applied to the depositional features, and that of Hernández-Molina et al. (2006b); Hernández-Molina et al. (2014) and García et al. (2009) to the erosive features.

4. Results

The abyssal topography is generally characterized by a system of ridges and depressions with a rough N-S direction generated through the crustal accretion at the EPR (Anderson and Noltimier, 1973; Macdonald et al., 1996), subsequent lithospheric stretching (Buck and Poliakov, 1998) and thermal subsidence (Menard, 1959; Andrews, 1971), later modified by further fracturing of the basaltic substrate (Yubko, 2016). The resulting abyssal morphology thus displays relatively narrow, elongated ridges and basins or valleys (both typically with few to tens of km in width), with east and west oriented slopes (Figs. 1b, 3).

4.1. Distribution and characterization of sedimentary basins

Three different types of basins can be distinguished (Fig. 3): open elongated basins, enclosed basins and basins paralleling the base of seamounts and seamount chains. The open elongated basins are dominant, and appear as long and relatively wide (about 10–15 km) parallel features in between the N-S seafloor fabric in areas B4 and B6, as well as northern and southern area B2 (Fig. 3). The second most frequent type of basins develops paralleling seamounts and seamount chains. The main seamount chain shows a general NW-SE trend cutting that of the seafloor fabric, and is surrounded by a flexural moat in which the oceanic crust is sunken or depressed due to subsidence, as a result of the weight of the volcanic edifices (Koppers and Watts, 2010) (Fig. 3). These basins are wide (up to 25 km) and flat (typically 1.5–2°), annex to the sharp relief of one or various seamounts and connected with several N-S open basins. The last type of basins identified in our study area consists of comparatively narrower and enclosed interspersed valleys (5–10 km width), frequently surrounded by abrupt
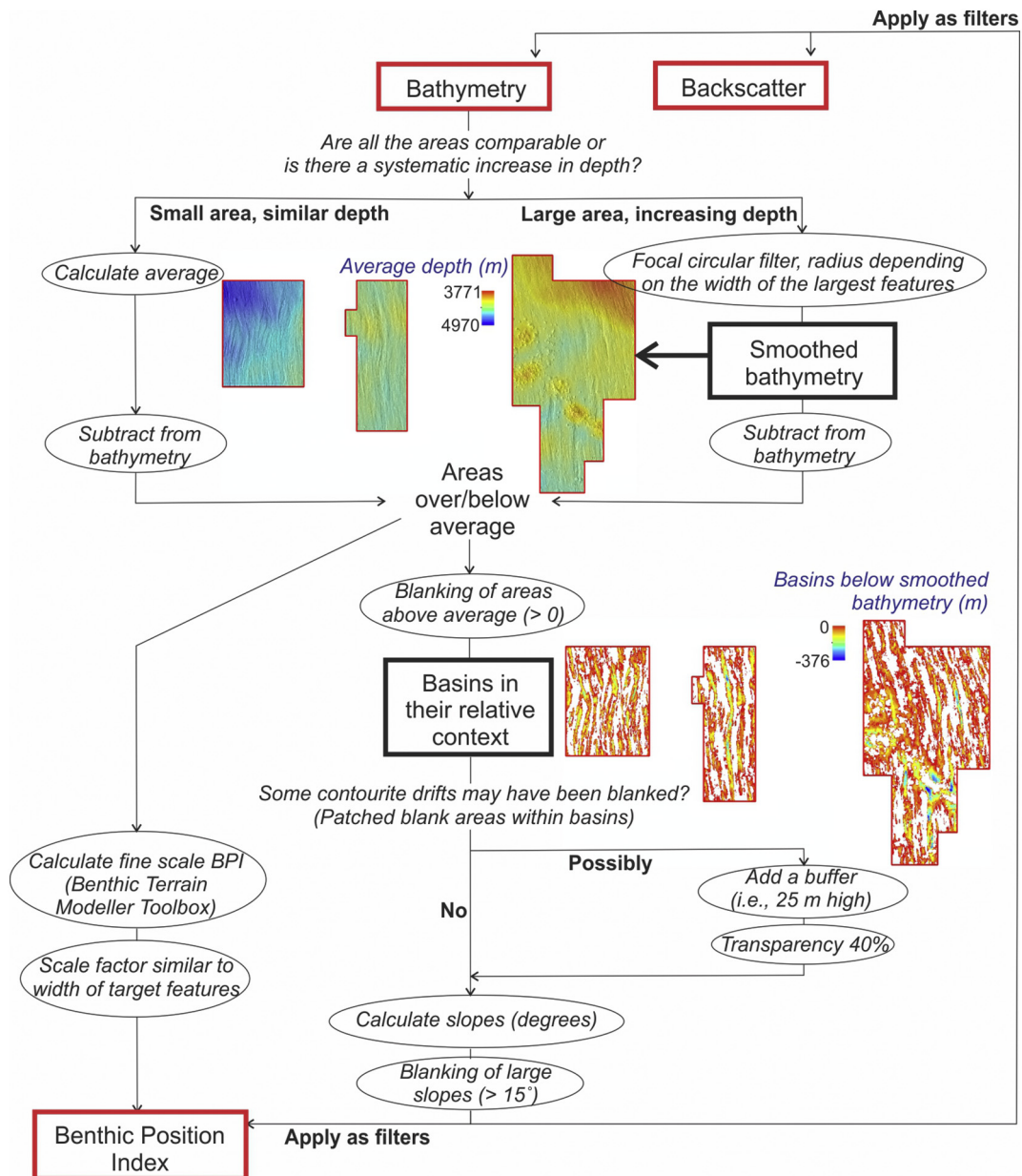
Fig. 2. Flow chart of followed processes in ArcGIS to generate the different maps and filters with the purpose of identifying the sedimentary basins, as well as to identify, evaluate and compare the main sedimentary features present within those basins.

escarpments (> 10°) and embedded between curved ridges in areas B2 and central area B4 (Fig. 3).

4.2. Main topographic obstacles

The topographic obstacles for bottom currents identified in the study area consist of isolated seamounts, seamount chains and elongated ridges. The regular ridges with a rough N-S direction dominate most of northern and southern area B2, area B4, and area B6 with a slightly curved NNW-SSE trend (Fig. 3). Standing out in this regular background topography, narrow and curved ridges (about 5 km wide) appear dominating the central parts of area B2 and B4, and a major and various minor seamount chains characterize area B6 (Fig. 3).

In the westernmost area (B2), the elongated ridges and depressions characterizing the seafloor are mostly oriented towards the NNW-SSE. The ridges progressively curve towards the east and increase their width and spacing holding deep enclosed basins in between, finally recovering sharply their original orientation. This sharp variation in the

trend of the seafloor fabric originates three sets of curved ridges and valleys with fusiform shape aligned in SW-NE direction (Fig. 3). The three fusiform, eye-shaped features range from 25 to 33 km in width and 80–100 km in length. The largest one is located in the SW end of the area B2, and the smallest one in the NE end (Fig. 3).

The central area (B4) is divided in two by a central deep depression with NNW-SSE trend, > 220 km long and > 100 m deeper than any other feature, being the largest basin in area B4 (Fig. 3). Up to 14 entwined or hummocky curved ridges stand out around 15°N due to their comparatively higher summits (~100 m), and maximum lengths of 60 km (Fig. 3). The hummocky ridges are typically grouped in sets of 3–5 curved ridges with NNW-SSE to NW-SE trend. The central deep depression appears curved paralleling the hummocky ridges at ~15°N, and its maximum depths (4750–4800 m) occur immediately north and south of this curved section, which is much shallower in comparison (4625 m) (Fig. 3).

In the easternmost area (B6) the regular seafloor fabric consisting of slightly curved NNW-SSE lineations are sharply cut by a NW-SE
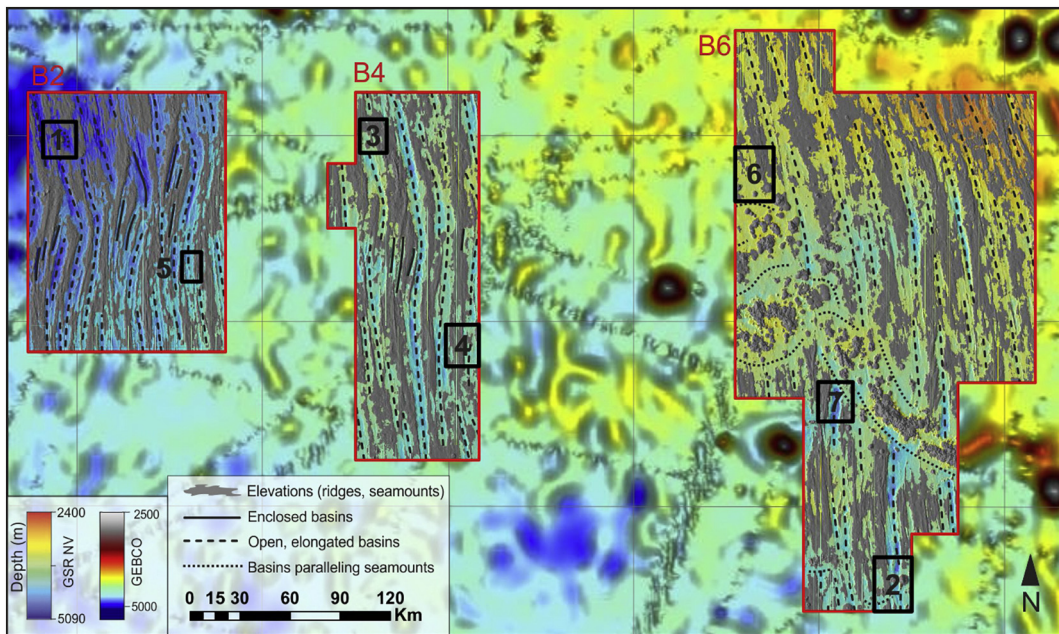
Fig. 3. Multibeam bathymetry with highs (ridges and seamounts) represented in grey colour in order to highlight the sedimentary basins. The highs are defined as those areas above the average within a radius of 15 km. The numbered areas marked in black correspond to Figs. 5, 6 and 7a,b. The source of the background bathymetric data is the General Bathymetric Chart of the Oceans (GEBCO). See Fig. 1a for location.
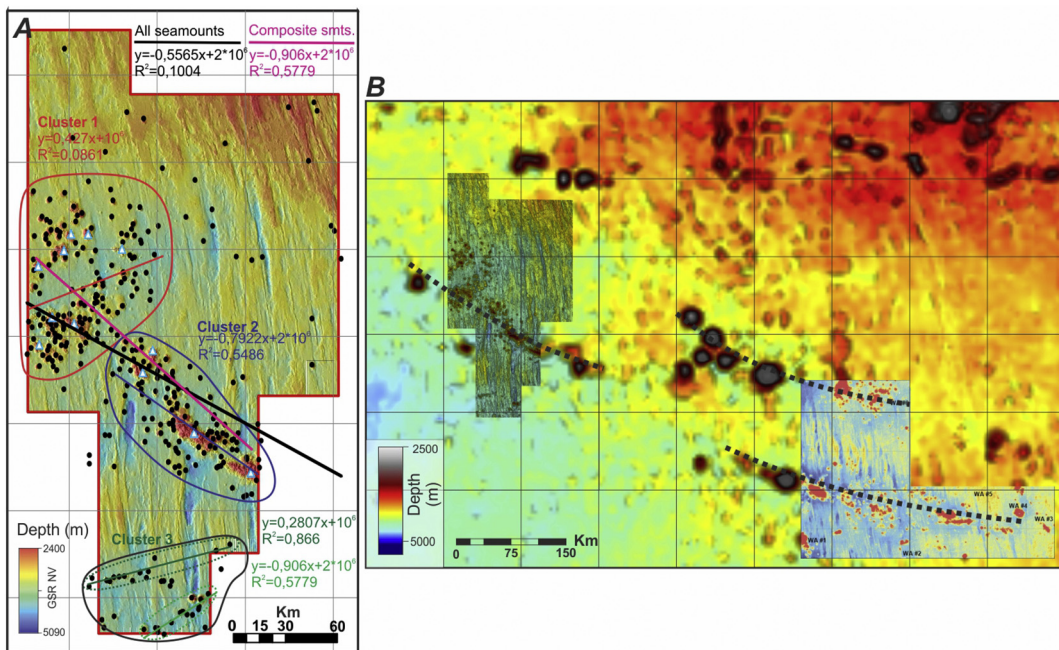

Fig. 4. A) Distribution of the seamounts observed in area B6 (white triangles represent composite seamounts, which are the spine of the main seamount chain; black dots represent isolated seamounts). Three clusters have been identified, with sub-clusters inside cluster 3. The fitted trend curve of each individual population or cluster has been calculated. B) General view of the seamounts located east of the study area (zone B6, see Fig. 1b for the uninterpreted bathymetry), allowing to observe the continuity of the seamount lineations (indicated with a black dashed line) in area the GEBCO bathymetry and in the German License Area (bathymetry from Rühlemann et al. (2011) and Mewes et al. (2014)).

seamount chain as well as various minor seamount chains (Fig. 4a). The identification, quantification and outline of seamounts (> 1000 m), knolls (200–1000 m) and highs (< 200 m) allowed to identify a total amount of 338 positive structures (Fig. 4a). Two main categories of seamounts have been established: overlapping multiple peaks (composite elevations) with large area and height and a width/length ratio below 0.8, and isolated elevations are characterized by a more circular form, with a width/length ratio higher than 0.8. Only twelve of these positive structures fit in the first category (Fig. 4a).

The distribution of all the elevations shows a very weak internal correlation, but the composite seamounts, which are the spine of the seamount chain, show a clear NW-SE trend (Fig. 4a). In addition, three main clusters are present: two of them are located close together (clusters 1 and 2), and the third one is located to the south (cluster 3) of area B6. The cluster 1 is located NW of B6 area, and is characterized by some of the smaller composite seamounts and a wide distribution of

small to large knolls with very weak internal correlation (Fig. 4a). The cluster 2 has a more compact distribution along its trend line towards the southeast, and consists of small to large knolls, as well as the largest composite seamounts (Fig. 4a), suggesting a more localized volcanic activity. The cluster 3 contains mostly small knolls in two smaller and well aligned ESE-WNW sub-clusters (Fig. 4a). The variations in the orientations of the southern cluster suggest other factors than plate movement influencing the distribution of seamount chains and the intensity of the volcanic activity.

Despite the fact that the observed seamounts seem to be grouped in several clusters (Fig. 4a), their combined general trend follows a northwest-southeast axis, which is consistent with the current trend of the Pacific plate (Smoot and Choi, 2003) and oblique compared to the orientation of the elongated abyssal hills (Tracey et al., 1971; Barckhausen et al., 2013). The available multibeam bathymetry, the GEBCO bathymetry and published data of similar seamount complexes described in the literature (Rühlemann et al., 2011; Mewes et al., 2014; Mewes et al., 2016) (Fig. 4b) have been combined to obtain a broader picture of the seamounts in the area: the lineation of seamounts in area B6 extends towards the ESE building various large-scale seamount chains hundreds of kilometres long (Fig. 4b), which are either aligned or follow a parallel trend.

4.3. Evidence of bottom-current controlled sedimentation

Several morphological features located within the sedimentary basins in the study area suggest the presence of bottom currents, discarding a pure pelagic or hemipelagic sedimentary regime. These morphological features show characteristics of small-sized contouritic drift features (Faugères et al., 1999; Hernández-Molina et al., 2006b; García et al., 2009; Hernández-Molina et al., 2014; Rebesco et al., 2014), and include a) depressions of about 20–100 m deep with a U-shaped cross-section and located at the base of seamounts, corresponding to *contourite moats*, or along the base of abrupt slopes, interpreted as *linear moats*; b) presumably erosive features < 20 m deep with a V-shaped cross-section and preferentially clustered at the base of a seamount (*furrows*) or c) located within a larger depression or valley (*abyssal sinuous channels*); d) mounded features plastered against a ridge or a slope have been classified as *plastered drifts*; e) mounded features with asymmetric cross-section and separated from the base of a slope by a moat (with the part with largest relief located alongside the moat) have been identified as *elongated separated drifts*; last, f) those elongated fan-like lobes formed in an comparatively unconfined basin after passing a gap have been classified as *abyssal contourite fans*. These features have been detected combining multibeam bathymetry, backscatter data, slope and bathymetric position index (BPI) (Weiss, 2001; Verfaillie et al., 2007; Wright et al., 2012) (Fig. 2). The different examples provided here for moats (Figs. 5, 7), linear moats (Figs. 6, 7b), furrows (Fig. 5), abyssal sinuous channels (Figs. 6, 7), plastered drifts (Fig. 5, inset 2; Fig. 6), elongated separated drifts (Fig. 5, inset 1; Fig. 6, inset 4; Fig. 7, inset 6) and abyssal contourite fans (Fig. 8) have been singled out based on three criteria: to include features present in the three areas (B2, B4 and B6), within various contexts (i.e., related to different types of features) and to evaluate different possible diagnosis criteria in the bathymetric, backscatter, and BPI maps.

Due to their scale, the U-shaped features, which reach hundreds of metres to few kilometres in width, are easily located in the multibeam map. Contrastingly, the V-shaped morphological features (which reach tends of metres to few hundred metres in width) are difficult to identify unless they are clustered near a seamount. Associated small-sized elongated features (Fig. 5, inset 1; Figs. 6, 7, inset 6; Fig. 8, inset 7) are possibly current-related features, but require further examination to confirm or deny this hypothesis. According to the backscatter dataset, light backscatter areas (low reflectivity) are frequent within the basins suggesting softer sediment, but they do not appear in direct association to the mounded features. On the opposite, areas with darker backscatter

(high reflectivity) show a good correlation to the axis of U and V-shaped negative features, suggesting the presence of a rougher or coarser seabed composition in association with these features (Figs. 5–7) (Mulder et al., 2003; Hernández-Molina et al., 2008b). The BPI dataset largely contributes in identifying the U and V-shaped features due to their concave shape (below −15 BPI). Additionally, the U-shaped depressions show values indicating their flat bottom (between −15 and 75). On the other hand, the BPI dataset also contributes in identifying convex sediment deposits characterized by quite homogeneous values over 75 BPI, which indicates their homogeneously smooth surface (Figs. 5–7).

As a result of applying the aforementioned diagnostic criteria, various examples of contouritic features appear associated to nearby seamounts (Fig. 5), ridges (Fig. 6), or within the axis of the valleys (Figs. 7, 8). The features associated with seamounts comprise U-shaped negative features around the seamount about 1–1.5 km wide and typically between 25 and 50 m deep but reaching depths up to 80 m. Fig. 5 (inset 1) gives an example, observed in area B2, in which two curved moats with rough N-S trend embrace a large knoll. The moat on the west is better developed reaching 80 m deep and 10.5 km long; the moat in the east is about 50 m deep and 8 km long (Fig. 5, inset 1). Small-sized elongated morphologies (about 5–15 km long), characterized by a smooth surface and convex shape appear attached to each U-shaped moat, with a maximum width of 2 km and 9.5 km in length alongside the largest moat and 1.5 km wide and about 5 km long alongside the smallest (Fig. 5, inset 1). Isolated V-shaped features are also present in the same area (10–15 m deep, < 5 km long), surrounding a small-scale ridge and characterized by streaks of dark backscatter and concave shape (Fig. 5, inset 1). Last, clustered V-shaped features of metric to decametric scale (up to 20 m deep) and reaching up to 200 m wide also appear associated to seamounts (Fig. 5, inset 2). The most outstanding example in the study area is found in southern area B6, where two knolls are embraced to the east by a curved depression with clustered deeper lineations; these lineations do not appear as continuous features, but as a succession of short scours of 0.5–2 km long and tens to a few hundred metres wide (Fig. 5, inset 2).

The features associated with ridges (Fig. 6, insets 3 and 4) consist of deep (50–100 m), elongated (about 5–15 km), rectilinear U-shaped moats running parallel to a partly exhumed ridge with an abrupt slope (> 15°). These linear moats associated with a ridge stand out because only one flank of the ridge is incised, acquiring a highly asymmetrical profile. Two examples have been singled out in area B4 (Fig. 6), but also appear in area B2 (Fig. 7, inset 5) and in area B6 (Fig. 7, inset 6). The northernmost example (Fig. 6, inset 3) reaches 10.5 km long and 90 m deep, with a short thalweg on its southern half. The southernmost example shows two linear moats, one reaching 10 km long and 65 m deep, and the second only reaching 5 km long and 55 m deep (Fig. 6, inset 3). The linear moats identified within this context (Fig. 6, insets 3 and 4) typically show light backscatter (low reflectivity) and darker backscatter (high reflectivity) immediately next to the ridge slope, suggesting increased sediment roughness. These linear moats are in turn associated to narrow and long sediment bodies (10 km long, 1.5 km wide) plastered against another ridge when present (Fig. 6), or to mounded sediment bodies (45 m high, 3.5 km wide, and 4.5 km long) when a wide valley allows its growth (Fig. 6, inset 4). Additionally, a mounded morphology of 7 km length and 3.5 km width with homogeneous convex shape and not associated to a ridge (Fig. 6, inset 3) has been identified.

Finally, those features located within valleys have been classified as such due to their location at the central axis of a valley or due to the interaction with the edges of the valley which are not characterized by an abrupt slope (> 15°). The main feature within the valley can be either U and V-shaped sinuous negative features (Fig. 7), or mounded depositional morphologies (Fig. 8). Abyssal sinuous V-shaped features reach about 10 km long and about 10 m deep (Fig. 7, inset 5). In a more complex sedimentary system, this V-shaped negative feature can evolve
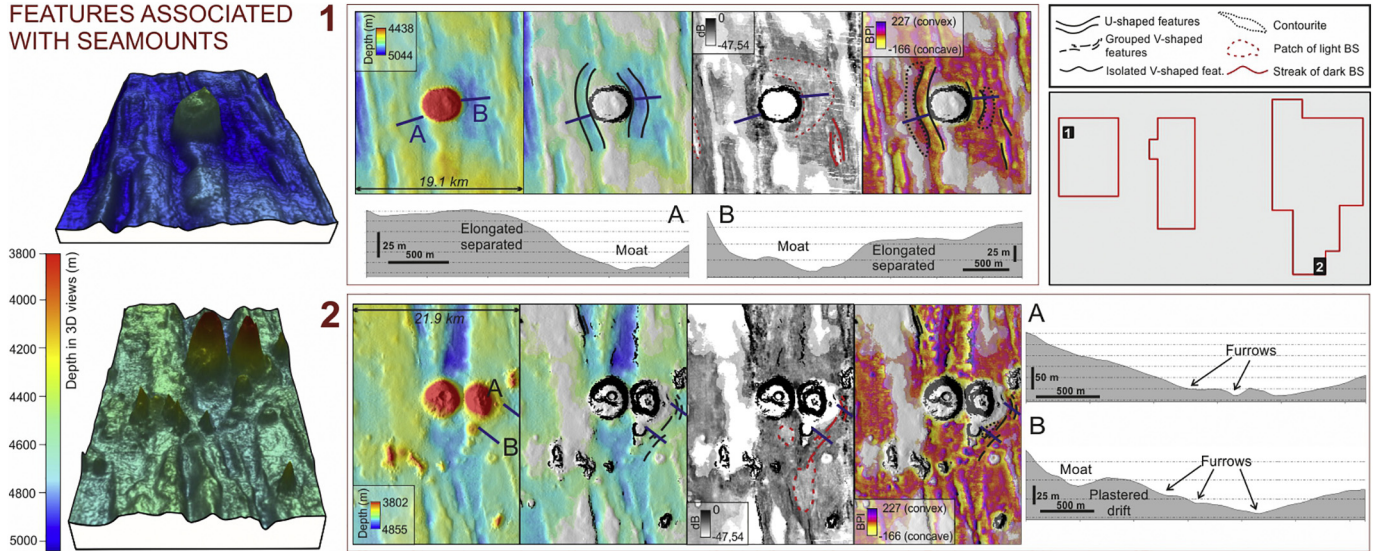
Fig. 5. Multibeam bathymetry, masked bathymetry, backscatter (BS) and bathymetric position index (BPI) of various basin areas near seamounts (zones 1 and 2; see Fig. 3 for location), together with bathymetric profiles in which erosive (furrows and moats) and depositional bottom current features have been identified. All the areas with positive mean elevations (> 0 m) in a 15 km radius are masked to cover the ridges and seamounts: the positive values between 0-25 m have colored in grey; all values over 25 m have been fully blanked.

to an U-shaped feature (25 m deep, 400–500 m wide) and present annex small-sized mounded sedimentary bodies (0.5–1 km wide, 6.5 km long and 15–20 m high) (Fig. 7, inset 6). These sinuous U and V-shaped depressions can be clearly observed in the backscatter dataset due to their darker backscatter (higher reflectivity), suggesting increased sediment roughness (Fig. 7) (Mulder et al., 2003), and can be flanked by patches of light backscatter (low reflectivity) which may be correlated with depositional features distributed in a patchy pattern (Fig. 7, inset 6). When mounded sedimentary bodies form fan-like features along a comparatively unconfined basin after the presence of a gap or gateways (thus representing a type of channel-related drift), linear moats appear running along the borders of the valley and surrounding the fan-like features, indicating erosion of previous fan drifts. This leads to the development of complex morphologies, with confined (6.5 km long, 1–2.5 km wide and 30–60 m high) and asymmetrical deposits (7 km long 3 km wide and about 40 m high) associated to various linear moats

(Fig. 8). In this last example, the backscatter has demonstrated to be correlated with the distribution of the various features, showing light backscatter over the sedimentary bodies and dark backscatter along the axis of the aforementioned linear moats (Fig. 8). The BPI provides a useful tool to delimit the boundaries for the delimitation of the borders of each feature (Fig. 8).

5. Discussion

5.1. Past and present geodynamic framework and its role on the distribution and morphology of the sedimentary basins

The evolution of the geodynamic framework has created several large-scale features (over 10 km in length or 200 m in relief) that nowadays characterize the study area, comprising N-S to NNW-SSE oriented ridges, sets of entwined curved ridges and enclosed basins, as
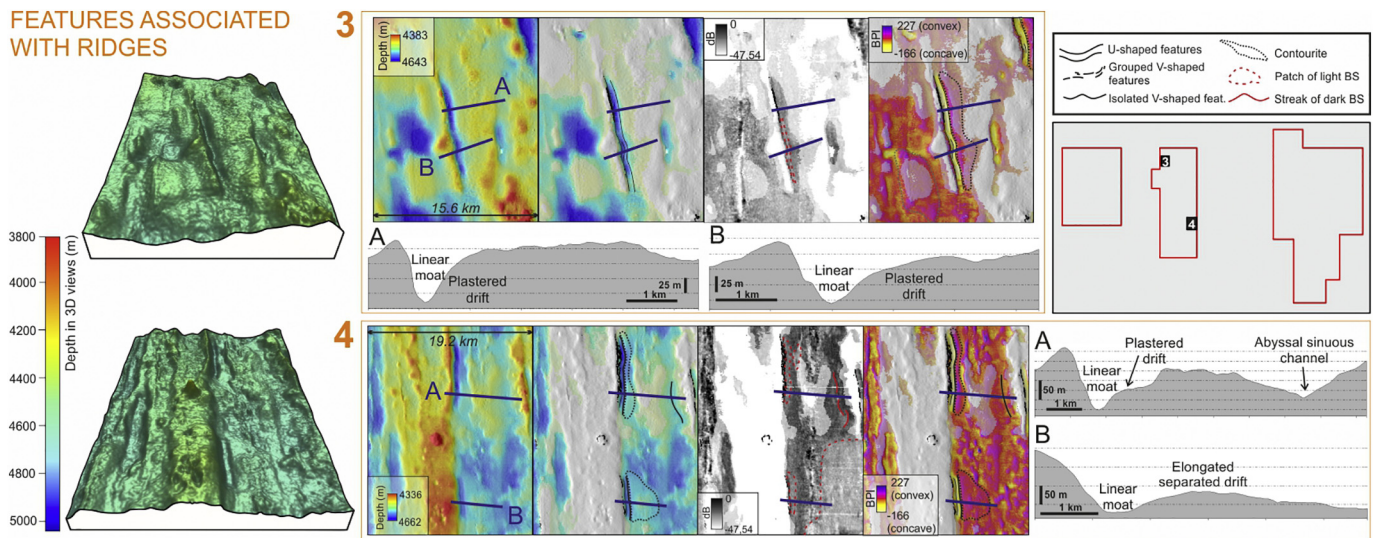

Fig. 6. Multibeam bathymetry, masked bathymetry, backscatter (BS) and bathymetric position index (BPI) of various basin areas near ridges (zones 3 and 4; see Fig. 3 for location), together with bathymetric profiles in which erosive (furrows and moats) and depositional (sediment drifts) bottom current features have been identified. All the areas with positive mean elevations (> 0 m) in a 15 km radius are masked to cover the ridges and seamounts: the positive values between 0-25 m have colored in grey; all values over 25 m have been fully blanked.
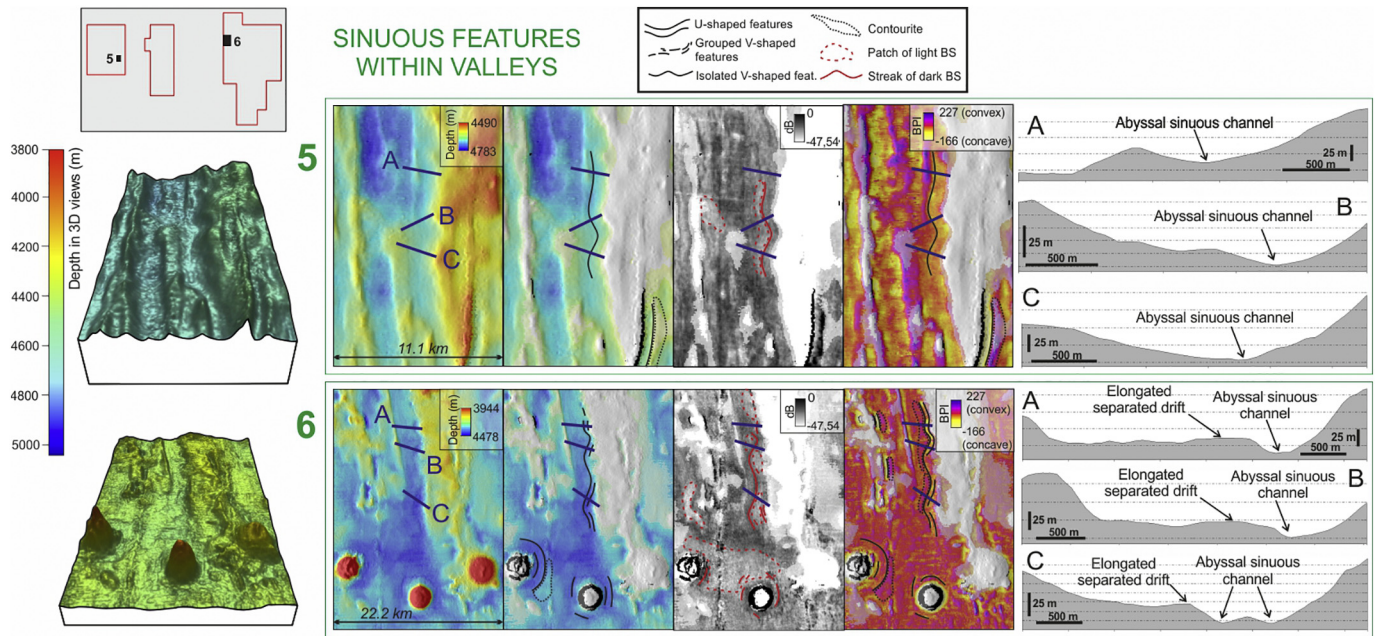
Fig. 7. Multibeam bathymetry, masked bathymetry, backscatter (BS) and bathymetric position index (BPI) of various basin areas within valleys (zones 5 and 6; see Fig. 3 for location) characterized by the presence of sinuous features, together with bathymetric profiles in which erosive (furrows and moats) and depositional (sediment drifts) contourite features have been identified. All the areas with positive mean elevations (> 0 m) in a 15 km radius are masked to cover the ridges and seamounts: the positive values between 0-25 m have colored in grey; all values over 25 m have been fully blanked.

well as aligned seamount chains, which are capable of deflect bottom currents and enhance their effect on the seafloor morphology.

The seafloor fabric originated at the axis of the Mathematicians Ridge between 24 and 33 Ma ago (Müller et al., 2008) due to the cyclic growth of the lithosphere at the axis of the EPR. The three eye-shaped tectonic structures identified in area B2 and the entwined hummocky ridges crossing area B4 at ~15°N are contemporaneous to the formation of the regular seafloor fabric and show strong similarities with the relict trace that could sculpt an Overlapping Spreading Center (OSC), and thus would originate at the same time as the regular seafloor fabric. OSCs tend to form in the coldest parts of fast-spreading zones that break into various segments (Macdonald et al., 1984; Macdonald et al., 1986), and appear due to the overlap of two *en échelon* ridge segments not connected by transform faults (Macdonald et al., 1984; Sempere et al., 1984; Macdonald et al., 1986). Several episodes of overlap can give rise to a large-scale trail of topographic anomalies present in older lithosphere, which can appear as linked hummocky structures with abandoned basins in between (Sloan, 1991; Carbotte and Macdonald, 1992; Ruellan et al., 1994; Cormier et al., 1996; White et al., 2009). The size

of the three identified eye-shaped structures is in the range of the features that would be generated by an OSC, and their morphology has a good correspondence with the model developed by Cormier et al. (1996) for right-stepping OSCs during a phase of northwards migration. According to this interpretation, the Mathematicians Ridge was composed of at least two ridge segments with a right-stepping OSC.

The seafloor fabric was later modified and enhanced by the combined effects of stretching of the lithosphere and thermal subsidence, as well as intraplate volcanism. The observed seamounts comprise various clusters (Fig. 4a) with a general trend that follows a northwest-southeast axis, consistent with the current trend of the Pacific plate (Smoot and Choi, 2003). These seamounts extend towards the ESE building various large-scale seamount chains hundreds of kilometres long (Fig. 4b). The formation of multiple thin plumelets detached from the top of a superplume in a closely spaced area frequently results in *en échelon* seamount trails as well as intermittent hotspot volcanism (Koppers et al., 2003).

All these positive features are accompanied by basins of various scales. Three different types of basins can be distinguished according to
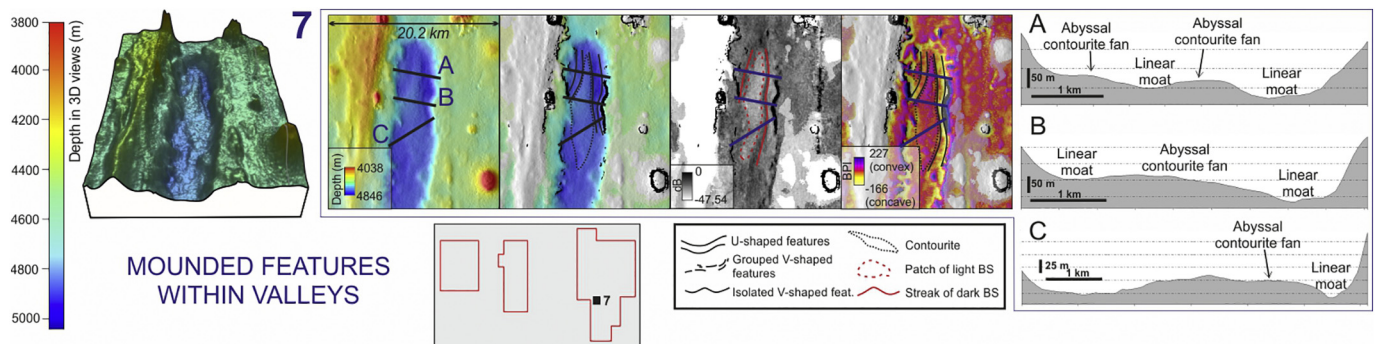

Fig. 8. Multibeam bathymetry, masked bathymetry, backscatter (BS) and bathymetric position index (BPI) of various basin areas within valleys (zone 7; see Fig. 3 for location) characterized by the presence of mounded features, together with bathymetric profiles in which erosive (furrows and moats) and depositional (sediment drifts) contourite features have been identified. All the areas with positive mean elevations (> 0 m) in a 15 km radius are masked to cover the ridges and seamounts: the positive values between 0-25 m have colored in grey; all values over 25 m have been fully blanked.

their origin and morphological context. The most abundant basins are relatively wide, N-S elongated basins located in northern and southern area B2 as well as most areas B4 and B6 originally formed in the spreading centre, flanked by ridges at both sides and open to the north and the south (Fig. 3). The second most frequent type of basins are those generated at the base of the seamounts (flexural moat) (Koppers and Watts, 2010) paralleling the seamount chains with a general NW-SE trend (Fig. 3), formed in a later period as a result of volcanic activity and interrupting the original seafloor fabric. These basins are typically wide, flat and well-connected with several N-S elongated basins. Last, narrow enclosed or partly enclosed curved or fusiform basins appear interspersed in between those entwined curved features that have been interpreted as an OSC relict trail (and thus also formed in the spreading centre) (Fig. 3).

5.2. Influence of the seafloor morphology on the basin sedimentation

The topographic obstacles have a crucial effect on the intensity and orientation of bottom currents (Roden, 1987; Stow et al., 2002b; Hunter et al., 2007; Faugères and Stow, 2008; Hernández-Molina et al., 2008b; Rebesco et al., 2014). The particular height and dimensions of the volcanic chains and isolated volcanic highs determines the degree to which bottom currents are accelerated and deflected around them up to doubling the bottom current velocity in the immediate area (Roden, 1987). Frequently the seamounts show scours or moats around their bases (Fig. 6, insets 1 and 2) (McCave and Carter, 1997; Van Rooij et al., 2007; García et al., 2009; Palomino et al., 2011; Vandorpe et al., 2014), but can also function as a protective topographical barrier against erosion (Skornyakova and Murdmaa, 1992) and create sediment accumulations at the lee side (McCave and Carter, 1997; Hernández-Molina et al., 2006a; Vandorpe et al., 2016). The linear obstacles (i.e., ridges) tend to generate current branches flowing along their base, frequently leading to erosional features (Hernández-Molina et al., 2008a) (Fig. 6, insets 3 and 4).

The shape and orientation of the basins, as well as their context, is also determinant to understand their interaction with the flow regime. The water masses are more easily funnelled through those basins with open ends and located near an obstacle capable of enhancing the local bottom current regime (i.e., basins with a similar orientation to that of the flow and located near a seamount; Van Rooij et al. (2010)) generating better developed and more complex sedimentary products (confined and elongated separated drifts, moats, linear moats, furrows and abyssal sinuous channels) (Fig. 8 inset 7). On the opposite, bottom-current features will be less favoured within the partly-enclosed valleys related to the OSC relict trail, despite their narrowness may also funnel the otherwise sluggish currents possibly diminishing the sedimentation rates. Considering all the evidences provided by the erosive and depositional contourite features within the study area, the basin fill sedimentation regime appears to dominate over the sediment drape, in agreement with the findings of Dubois and Mitchell (2012).

5.3. Dynamics of the abyssal currents in the study area

The action of bottom currents had been suggested to affect the sedimentary regime in the central Pacific seafloor only during cold periods of intensified circulation (Johnson, 1972; Pautot and Melguen, 1975; Van Andel et al., 1975; Lonsdale and Spiess, 1977; Lonsdale, 1981; Mangini et al., 1982; Nishimura, 1992), with few exceptions providing proof of present-day contourite features (Beiersdorf, 1987; von Stackelberg and Beiersdorf, 1991; Dubois and Mitchell, 2012). Now, the presence of contourite features in the study area demonstrates the action of bottom currents locally sculpting the seafloor, and provides new tools to deduct their general averaged direction and character. Thus, an in-detail analysis of the complexity of the abyssal circulation, which is linked to the underlying bathymetric relief and the surface tides (Polzin et al., 1997), is beyond this study. For that, the

enhancement of a current branch in response to the Coriolis effect (to the right in the northern hemisphere) provides a tool to deduct the direction of the general averaged circulation (Faugères et al., 1999), despite this effect is weaker at low latitudes.

The scale of the contourites identified in the central Pacific ocean at abyssal depths contrasts with that of abyssal contourite features previously described in the literature, which mostly consist of extensive contourite sheets located near the continents (Hernández-Molina et al., 2008a), with hundreds of kilometres in length (i.e., Hikurangi fan drift, Carter and McCave, 2002; Greater Antilles Outer Ridge, Tucholke, 2002). In contrast, their size is similar to that of contourites typically developed along continental margins, with < 100 km long (i.e., the Faro-Albufeira drift, Stow et al., 2002c; Porcupine Seabight drifts, Van Rooij et al., 2007) although exceptionally extensive drifts are also present in this environment (i.e., the Eirik drift, Hunter et al., 2007).

The western area (B2) has few contourite features, being those examples provided in this study (Fig. 5, inset 1; Fig. 7, inset 5) some of the few elements evidencing the action of bottom currents affecting the sedimentation pattern. In the case of the two moats surrounding the knoll (Fig. 5, inset 1), the deepest, longest and better developed one lies on the western side of the knoll. When the impinging bottom flow is separated into two branches due to the presence of an obstacle, the effect of the Coriolis force enhances the left branch of the seamount on the northern hemisphere (Hernández-Molina et al., 2008b; Zenk, 2008). Thus, we can infer the dominance of a northwards directed flow (Fig. 9).

In the central area (B4) (Fig. 6) both examples show linear moats eroding the eastern flank of elongated ridges. The enhancement of the left branch caused by the Coriolis effect in the northern hemisphere suggests that in this case, the dominant flow has a dominant southwards component (Fig. 9), further exhuming the annex ridge and redepositing the sediment on the opposite side due to the helicoidal flow within the linear moat, favouring the growth of a contourite drift (Faugères and Stow, 2008).

Last, in the southern part of area B6 the evidences of the action of the bottom currents appear as grouped furrows sculpted east of the knolls (Fig. 5, inset 2) and suggesting a southward flow (Fig. 9). In the central area B6 (Fig. 8, inset 7), the presence of a confined drift suggests that both a northward and a southward flow can occur, sculpting each of the linear moats embracing the drift, but the better development of the eastern linear moat with an elongated separated drift on its southern end indicates a slightly stronger or more frequent northwards flow (Faugères et al., 1999) (Fig. 9). In northern area B6 (Fig. 7, inset 6), a sinuous erosive feature sculpted against the eastern wall of a valley with patchy contourite deposits along its path indicates a dominant northwards flow.

These apparently contradicting flows (Fig. 9) reveal information on the dynamics governing the study area and the development of the contourite drifts, suggesting a variable flow with two dominant regimes, northwards and southwards, that are locally enhanced depending on the morphological context. The higher variability of flow dynamics revealed by the contourite drifts present in area B6 may result from the presence of the seamount chain: the higher roughness has been demonstrated to impact on the spatial distribution of the pycnocline, diffusivity and velocity field of a flow even hundreds of metres above the seafloor (Polzin et al., 1997; Zenk, 2008; Zhang et al., 2017).

According to the moorings recorded within the study area, the average flow sweeping the seafloor already appears as variable, in average directed to the SW (M1, Table 1) (Amos et al., 1977), the W (M2, Table 1) (Morgan et al., 1999), and NW with periodical shifts to a S flow (M3, Table 1) (Hayes, 1979; Hayes, 1980). Internal waves and tidal waves were also detected (Amos et al., 1977; Hayes, 1980) within the study area, and the action of benthic storms has been recorded west of the study area (Demidova et al., 1993; Morgan et al., 1999). All these mooring data confirm the existence of a variable flow in which both the northwards-directed LCPW and the southwards-directed NPDW may
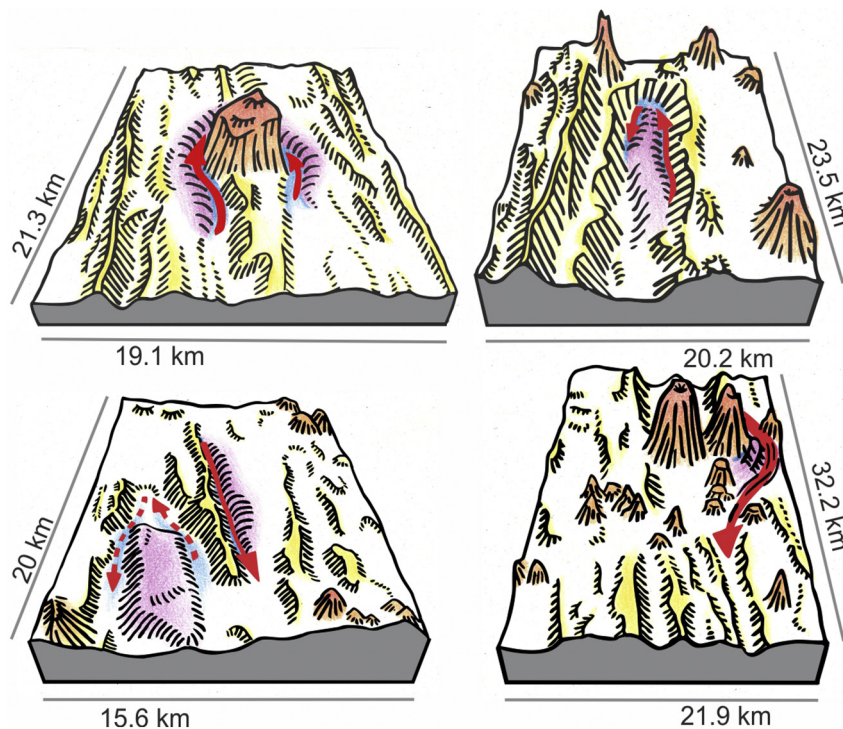
Fig. 9. 3D sketch of the areas depicted in Fig. 5, inset 1 (top, left), Fig. 4, inset 3 (bottom, left), Fig. 8, inset 7 (top, right) and Fig. 5, inset 2 (bottom, right). The orange colours represent abyssal highs and knolls; the yellow colours represent narrow ridges and escarpments; the purple colours represent inferred contourite depositional features; the blue colours represent inferred contourite erosive features. The red arrows represent the inferred general, averaged path of the bottom currents.

interact. The areas in which LCPW and NPDW interact have been suggested to endure seasonal and decadal changes depending on climatic fluctuations (Hayes, 1980; Halbach et al., 1988), which may manifest as longitudinal variations of the boundary. In addition, the different density of both water masses causes part of NPDW to flow over a wedge of LCPW (Mitchell et al., 2003). These conditions would favour the presence of a relevant pycnocline along which tidal and internal waves can develop (Shanmugam, 2014) and ultimately interact with the seafloor. Additionally, internal waves and tides can be expected to travel 100 km away from their generation site before being scattered by the action of topography, and up to 1000 km if generated by large features (St Laurent and Garrett, 2002), what makes it possible for the internal waves and tides acting in the study area to result from the hindrance to the northwards LCPW flow caused by the Clipperton FZ (Johnson, 1972; Jeong et al., 1994) and to the southwards NPDW flow caused by the Clarion FZ.

Overall, all flow information deduced from the inferred contourite deposits (Fig. 9), from current metres within the study area (Table 1) and according to previous studies (Amos and Roels, 1977; Amos et al., 1977; Gardner et al., 1984; Morgan et al., 1999), the bottom flow appears to be largely influenced by the action of internal waves and tides (baroclinic currents), occasionally affected by variations of the boundary between LCPW and NPDW and high-energy events related to benthic storms (Gardner and Sullivan, 1981; Demidova et al., 1993; Morgan et al., 1999). In turn, this tidal regime appears to be locally redirected and enhanced due to the N-S trend of the seafloor fabric and the gaps along the seamount chain (Roden, 1987; Zhang et al., 2017).

5.4. Relationships between bottom-currents and ferromanganese nodules in the CCZ

The variations in backscatter described in the studied areas are linked to the roughness of the terrain (i.e., bare rock, rocky fragments) and to the softness of the sediment, in place modulated by more focused bottom current flow. Given that the CCZ is widely known for the presence of ferromanganese nodules (Price and Calvert, 1970; Margolis and Burns, 1976; Bischoff and Piper, 1979; Glasby et al., 1982; Halbach et al., 1988; Hoffert, 2008, among many others), which is also the

rationale behind the exploration within our study area, we can tentatively suggest that the presence of nodules may be the cause behind the roughness of the seafloor (Rühlemann et al., 2011). The environmental parametres linking oceanography and ferromanganese nodule growth have been approached from many views and disciplines (Price and Calvert, 1970; Pautot and Melguen, 1975; Glasby, 1978; Nishimura, 1992; Jeong et al., 1994; Kasten et al., 1998; Han et al., 2003; González et al., 2010, 2012, 2016). On the other hand, the linkage between contourite drifts and nodule coverage and facies has been explored in few works (Beiersdorf, 1987; von Stackelberg et al., 1987; von Stackelberg and Beiersdorf, 1991; Wright et al., 2005). Under the assumption of the presence of nodules in our study area, the streaks and patches of dark backscatter that are coincident with moats (Fig. 5, inset 1), linear moats (Fig. 8), abyssal sinuous channels (Fig. 7) and furrows (Fig. 5, inset 2) could be indicative of the presence of nodules. These nodules may be exhumed due to the higher intensity of the flow, as previously described in contourite channels located in other settings (González et al., 2010, 2012, 2016). On the opposite, most examples of contourite drifts described here are coincident with patches of light backscatter (Figs. 5, 7, 8), suggesting the presence of soft sediment.

In a setting with rough bathymetry the current-related features are more likely to be found within basins with open ends (Fig. 3) and a similar orientation to that of the flow (Figs. 7 and 8), as well as near obstacles capable of enhancing the local bottom current regime such as seamounts (Fig. 5) and linear obstacles (Fig. 6). Assuming that the areas with medium to high backscatter correlate with rough seafloor due to the presence of ferromanganese nodules (Rühlemann et al., 2011) and according to the findings of this study (Figs. 5 to 8), ferromanganese nodules are likely to be found within elongated erosive features (moats, linear moats, sinuous channels and furrows), which are typically located bordering contourite drifts. The specific setting in which contourite drifts develop in the abyssal areas within the CCZ (Figs. 3, and 5 to 8), together with the contrast between the light and dark backscatter of the contourite drifts and annex erosive features (Figs. 5 to 8) will cause the occurrence of the nodule fields to be far more patchy than previously assumed. This will also be favoured by the variations in the distribution of nodules caused by environmental parameters (Kasten et al., 1998), such as variations in the sedimentation rates and burial of

organic matter, which in turn affects the diagenesis.

Despite the limitations of the available data, which due to the lack of seismic records only allows to identify current-related features with a positive (or negative) relief and only based on backscatter may mix up rocky outcrops and potential nodule fields, this work represents a new approach to understand the interaction of bottom currents and sedimentary dynamics in the eastern CCZ. Under the light of these findings, contourite research reveals as a tool with an interesting potential for ferromanganese nodule exploration.

6. Conclusions

The geological history of the study area is complex, which allows the presence of large-scale obstacles and sedimentary basins of various origins to coexist. The morphology and orientation of the obstacles has a direct influence on the sedimentary regime in the nearby sedimentary basins, due to the funnelling and acceleration of the deep-sea currents and the subsequent erosive, depositional or non-depositional regimes. The flow is most probably influenced by internal and tidal waves and high-energy events related to benthic storms (Gardner and Sullivan, 1981; Demidova et al., 1993; Morgan et al., 1999), redirected by the N-S trend of the basins and ridges present in the area (Menard, 1964; Rühlemann et al., 2011; Mewes et al., 2014). As a result, those basins bordered by ridges and located near topographic obstacles are more likely to hold bottom-current sedimentary products. Among these, erosive (moats, linear moats, furrows and abyssal sinuous channels) and depositional (patched plastered, elongated separated and confined drifts) contourite features have been identified (Dubois and Mitchell, 2012), evidencing the influence of the flow over the sedimentary regime. In addition, the varied morphologies of the contourites and the abundance of erosive features suggest the dominance of the basin fill sedimentation regime over the sediment drape regime (Dubois and Mitchell, 2012), which would favour the deposition of extensive sheeted drifts such as those observed in the abyssal plains (Hernández-Molina et al., 2008a). The small scale (< 100 km long) of the identified contourite features is comparable to that of contourites typically observed along continental margins (Stow et al., 2002c; Van Rooij et al., 2007; Hernández-Molina et al., 2008b) and contrasts with the large scale (hundreds of kilometres long) of the abyssal sheets (Carter and McCave, 2002; Tucholke, 2002; Hernández-Molina et al., 2008a).

Studies analysing the contourites present on the remote abyssal ocean floor are scarce (Beiersdorf, 1987; von Stackelberg and Beiersdorf, 1991; Dubois and Mitchell, 2012) and thus the knowledge of the interactions between secondary flows of the deep water masses is very limited. A bathymetric dataset only allows to detect those features with a positive relief (i.e., elongated separated, confined and plastered drifts), and the presence of other depositional contourites with no positive relief such as sheeted drifts may go unnoticed unless analyzed using seismic reflection profiles. Despite these limitations, the relevance of erosion and re-deposition, as well as the complexity of the seafloor features which develop in areas where bottom currents interact with tectonic an volcanic features has been demonstrated. Last, the patchy distribution of the current-related sedimentary bodies may affect the ferromanganese nodule occurrence, thus encouraging their study in areas with high interest for the mining industry.

Acknowledgements

References

Amos, A.F., Roels, O.A., 1977. Environmental aspects of manganese nodule mining. Mar. Policy 1, 156–163.

Amos, A.F., Roels, O.A., Garside, C., Malone, T.C., Paul, A.Z., 1977. Environmental aspects of nodule mining. In: Glasby, G.P. (Ed.), Marine Manganese Deposits. Elsevier, Amsterdam, pp. 391–437.

Anderson, R.N., Davis, E.E., 1973. A topographic interpretation of the Mathematician Ridge, Clipperton Ridge, East Pacific Rise system. Nature 241, 191–193.

Anderson, R.N., Noltimier, H.C., 1973. A model for the horst and graben structure of midocean ridge crests based upon spreading velocity and basalt delivery to the oceanic crust. Geophys. J. R. Astron. Soc. 34, 137–147.

Andrews, J.E., 1971. Abyssal hills as evidence of transcurrent faulting on North Pacific fracture zones. Geol. Soc. Am. Bull. 82, 463–470.

Barckhausen, U., Bagge, M., Wilson, D.S., 2013. Seafloor spreading anomalies and crustal ages of the Clarion-Clipperton Zone. Mar. Geophys. Res. 34, 79–88.

Batiza, R., 1982. Abundances, distribution and sizes of volcanoes in the Pacific Ocean and implications for the origin of non-hotspot volcanoes. Earth Planet. Sci. Lett. 60, 195–206.

Beiersdorf, H., 1987. Interpretation of seafloor relief and acoustic facies in the Clarion-Clipperton block southeast of Hawaii in terms of depositional, diagenetic, and tectonic processes. In: von Stackelberg, U., Beiersdorf, H. (Eds.), Manganese Nodules and Sediments in the Equatorial North Pacific Ocean. Geologisches Jahrbuch Reiche D 87, pp. 27–69.

Bischoff, J.L., Piper, D.Z., 1979. Marine Geology and Oceanography of the Pacific Manganese Nodule Province. Plenum Press, New York (842 pp).

Buck, W.R., Poliakov, A.N.B., 1998. Abyssal hills formed by stretching oceanic lithosphere. Nature 392, 272–275.

Carbotte, S., Macdonald, K., 1992. East Pacific Rise 8°–10°30′N: evolution of ridge segments and discontinuities from SeaMARC II and three-dimensional magnetic studies. J. Geophys. Res. Solid Earth 97, 6959–6982.

Carter, L., McCave, I.N., 2002. Eastern New Zealand Drifts, Miocene-recent. In: Stow, D.A.V., Pudsey, C.J., Howe, J.A., Faugères, J.-C., Viana, A.R. (Eds.), Deep-water Contourite Systems: Modern Drifts and Ancient Series, Seismic and Sedimentary Characteristics. Geological Society, London, Memoirs, pp. 385–407.

Cormier, M.-H., Scheirer, D.S., Macdonald, K.C., 1996. Evolution of the East Pacific Rise at 16°–19°S since 5 Ma: bisection of overlapping spreading centers by new, rapidly propagating ridge segments. Mar. Geophys. Res. 18, 53–84.

Craig, J.D., 1979. The relationship between bathymetry and ferromanganese deposits in the north Equatorial Pacific. Mar. Geol. 29, 165–186.

De Clippele, L., Gafeira, J., Robert, K., Hennige, S., Lavaleye, M., Duineveld, G., Huvenne, V., Roberts, J., 2017. Using novel acoustic and visual mapping tools to predict the small-scale spatial distribution of live biogenic reef framework in cold-water coral habitats. Coral Reefs 36, 255–268.

Demidova, T., Kontar, E., 1989. On the bottom currents in the area of development of ferrous manganese nodules. Dokl. Akad. Nauk SSSR 2, 468–472.

Demidova, T.A., Kontar, E.A., Sokov, A.V., Belyaev, A.M., 1993. The bottom currents in the area of abyssal hills in the north-east tropical Pacific Ocean. Phys. Oceanogr. 4, 53–61.

Demidova, T., Kontar, E., Yubko, V., 1996. Benthic current dynamics and some features of manganese nodule location in the Clarion-Clipperton Province. Oceanol. Russ. Acad. Sci. 36, 94–101.

Divins, D.L., 2003. Total Sediment Thickness of the World's Oceans & Marginal Seas 1. NOAA National Geophysical Data Center, Boulder, CO.

Dubois, N., Mitchell, N.C., 2012. Large-scale sediment redistribution on the equatorial Pacific seafloor. Deep-Sea Res. I Oceanogr. Res. Pap. 69, 51–61.

Faugères, J.C., Stow, D.A.V., 2008. Contourite drifts: nature, evolution and controls. In: Rebesco, M., Camerlenghi, A. (Eds.), Contourites, Developments in Sedimentology 60. Elsevier, Amsterdam, pp. 257–288.

Faugères, J.-C., Stow, D.A.V., Imbert, P., Viana, A.R., 1999. Seismic features diagnostic of contourite drifts. Mar. Geol. 162, 1–38.

Fisher, A.T., Wheat, C.G., 2010. Seamounts as conduits for massive fluid, heat, and solute fluxes on ridge flanks. Oceanography 23, 74–87.

Gafeira, J., Diaz, D., Long, D., 2015. Semi-automated mapping and characterisation of coral reef mounds: Mingulay Reef proof of concept. J. Interesting Things 1, 1–5.

Gao, Z., Eriksson, K.A., He, Y., Luo, S., Guo, J., 1998. Deep-water Traction Current Deposits: A Study of Internal Tides, Internal Waves, Contour Currents and Their Deposits. Science Press, Beijing.

García, M., Hernández-Molina, F.J., Llave, E., Stow, D.A.V., León, R., Fernández-Puga, M.C., Diaz del Río, V., Somoza, L., 2009. Contourite erosive features caused by the Mediterranean Outflow Water in the Gulf of Cadiz: Quaternary tectonic and oceanographic implications. Mar. Geol. 257, 24–40.

Gardner, W.D., Sullivan, L.G., 1981. Benthic storms: temporal variability in a deep-ocean nepheloid layer. Science 213, 329–331.

Gardner, W.D., Sullivan, L.G., Thorndike, E.M., 1984. Long-term photographic, current, and nephelometer observations of manganese nodule environments in the Pacific. Earth Planet. Sci. Lett. 70, 95–109.

Glasby, G.P., 1978. Deep-Sea manganese nodules in the stratigraphic record: evidence from DSDP cores. Mar. Geol. 28, 51–64.

Glasby, G.P., Stoffers, P., Sioulas, A., Thijssen, T., Friedrich, G., 1982. Manganese nodule formation in the Pacific Ocean: a general theory. Geo-Mar. Lett. 2, 47–53.

González, F.J., Somoza, L., Lunar, R., Martínez-Frías, J., Martín-Rubí, J.A., Torres, T., Ortiz, J.E., Díaz-del-Río, V., 2010. Internal features, mineralogy and geochemistry of ferromanganese nodules from the Gulf of Cadiz: the role of the Mediterranean Outflow Water undercurrent. J. Mar. Sci. 80, 203–218.

González, F.J., Somoza, L., León, R., Medialdea, T., Torres, T., Ortiz, J.E., Lunar, R., Martínez-Frías, J., Merinero, R., 2012. Ferromanganese nodules and micro-hardgrounds associated with the Cadiz Contourite Channel (NE Atlantic): palaeoenvironmental records of fluid venting and bottom currents. Chem. Geol. 310–311, 56–78.

González, F.J., Somoza, L., Hein, J.R., Medialdea, T., León, R., Urgorri, V., Reyes, J.,

Martín-Rubí, J.A., 2016. Phosporites, Co-rich Mn nodules, and Fe-Mn crusts from Galicia Bank, NE Atlantic: reflections of Cenozoic tectonics and paleoceanography. Geochem. Geophys. Geosyst. 17, 346–374.

Halbach, P., Friedrich, G., von Stackelberg, U., 1988. The Manganese Nodule Belt of the Pacific Ocean: Geological Environment, Nodule Formation, and Mining Aspects. F. Enke, Stuttgart.

Han, X., Jin, X., Yang, S., Fietzke, J., Eisenhauer, A., 2003. Rhythmic growth of Pacific ferromanganese nodules and their Milankovitch climatic origin. Earth Planet. Sci. Lett. 211, 143–157.

Hayes, S.P., 1979. Benthic current observations at DOMES Sites A, B, and C in the tropical north Pacific Ocean. In: Bischoff, J.L., Piper, D.Z. (Eds.), Marine Geology and Oceanography of the Pacific Manganese Nodule Province. Springer, US, pp. 83–112.

Hayes, S.P., 1980. The bottom boundary layer in the eastern tropical Pacific. J. Phys. Oceanogr. 10, 315–329.

He, Y., Duan, T., Gao, Z., 2008. Sediment entrainment. In: Rebesco, M., Camerlenghi, A. (Eds.), Contourites, Developments in Sedimentology 60. Elsevier, Amsterdam, pp. 99–119.

Heezen, B.C., Hollister, C., 1964. Deep-sea current evidence from abyssal sediments. Mar. Geol. 1, 141–174.

Heezen, B.C., Hollister, C.D., Ruddiman, W.F., 1966. Shaping of the continental rise by deep geostrophic contour currents. Science 152, 502–508.

Hein, J.R., Koschinsky, A., Halbach, P., Manheim, F.T., Bau, M., Kang, J.-K., Lubick, N., 1997. Iron and manganese oxide mineralization in the Pacific. In: Nicholson, K., Hein, J.R., Buhn, B., Dasgupta, S. (Eds.), Manganese Mineralization: Geochemistry and Mineralogy of Terrestial and Marine Deposits. Geological Society Special Publication, pp. 123–138.

Hernández-Molina, F.J., Larter, R.D., Rebesco, M., Maldonado, A., 2004. Miocene changes in bottom current regime recorded in continental rise sediments on the Pacific margin of the Antarctic Peninsula. Geophys. Res. Lett. 31, L22606.

Hernández-Molina, F.J., Larter, R.D., Rebesco, M., Maldonado, A., 2006a. Miocene reversal of bottom water flow along the Pacific Margin of the Antarctic Peninsula: stratigraphic evidence from a contourite sedimentary tail. Mar. Geol. 228, 93–116.

Hernández-Molina, F.J., Llave, E., Stow, D., García, M., Somoza, L., Vázquez, J., Lobo, F., Maestro, A., Díaz del Río, V., León, R., 2006b. The contourite depositional system of the Gulf of Cadiz: a sedimentary model related to the bottom current activity of the Mediterranean outflow water and its interaction with the continental margin. Deep-Sea Res. II Top. Stud. Oceanogr. 53, 1420–1463.

Hernández-Molina, F.J., Maldonado, A., Stow, D.A.V., 2008a. Abyssal plain contourites. In: Rebesco, M., Camerlenghi, A. (Eds.), Contourites, Developments in Sedimentology 60. Elsevier, pp. 345–378.

Hernández-Molina, F.J., Llave, E., Stow, D.A.V., 2008b. Continental slope contourites. In: Rebesco, M., Camerlenghi, A. (Eds.), Contourites, Developments in Sedimentology 60. Elsevier, pp. 379–408.

Hernández-Molina, F.J., Stow, D.A.V., Llave, E., Rebesco, M., Ercilla, G., Van Rooij, D., Mena, A., Vázquez, J.-T., Voelker, A., 2010. Deep-water Circulation: Processes & Products (Book of Abstracts). Sociedad Geológica de España, Baiona, Spain.

Hernández-Molina, F.J., Llave, E., Preu, B., Ercilla, G., Fontan, A., Bruno, M., Serra, N., Gomiz, J.J., Brackenridge, R.E., Sierro, F.J., Stow, D.A., Garcia, M., Juan, C., Sandoval, N., Arnaiz, A., 2014. Contourite processes associated with the Mediterranean outflow water after its exit from the Gibraltar Strait: global and conceptual implications. In: 2nd Deep-Water Circulation Congress, Ghent, Belgium, pp. 99–100.

Hernández-Molina, F.J., Wåhlin, A., Bruno, M., Ercilla, G., Llave, E., Serra, N., Rosón, G., Puig, P., Rebesco, M., Van Rooij, D., 2016. Oceanographic processes and morpho-sedimentary products along the Iberian margins: a new multidisciplinary approach. Mar. Geol. 378, 127–156.

Herron, E.M., 1972. Sea-floor spreading and the Cenozoic history of the east-central Pacific. Geol. Soc. Am. Bull. 83, 1671–1692.

Hoffert, M., 1980. Les Argiles rouges des grands fonds dans le Pacifique centre-est: authigenèse, transport, diagenèse. Institut de géologie. Université Louis Pasteur, Strasbourg, pp. 231.

Hoffert, M., 2008. Les nodules polymétalliques dans les grands fonds océaniques: une extraordinaire aventure minière et scientifique sous-marine. Vuibert, Paris.

Hollister, C.D., 1993. The concept of deep-sea contourites. Sediment. Geol. 82, 5–11.

Hollister, C., McCave, I., 1984. Sedimentation under deep-sea storms. Nature 309, 220–225.

Howe, J., 2008. Methods for contourite research. In: Rebesco, M., Camerlenghi, A. (Eds.), Contourites, Developments in Sedimentology 60. Elsevier, pp. 19–33.

Hunter, S.E., Wilkinson, D., Stanford, J., Stow, D.A.V., Bacon, S., Akhmetzhanov, A.M., Kenyon, N.H., 2007. The Eirik Drift: a long-term barometer of North Atlantic deep-water flux south of Cape Farewell, Greenland. In: Viana, A.R., Rebesco, M. (Eds.), Economic and Palaeoceanographic Significance of Contourite Deposits. Geological Society, London, Special Publications, pp. 245–263.

Jeong, K.S., Kang, J.K., Chough, S.K., 1994. Sedimentary processes and manganese nodule formation in the Korea Deep Ocean Study (KODOS) area, western part of Clarion-Clipperton fracture zones, northeast equatorial Pacific. Mar. Geol. 122, 125–150.

Johnson, D.A., 1972. Ocean-floor erosion in the Equatorial Pacific. Geol. Soc. Am. Bull. 83, 3121–3144.

Johnson, D.A., Johnson, T.C., 1970. Sediment redistribution by bottom currents in the central Pacific. Deep-Sea Res. I Oceanogr. Res. Pap. 17, 157–169.

Johnson, G.C., Toole, J.M., 1993. Flow of deep and bottom waters in the Pacific at 10°N. Deep-Sea Res. I 40, 371–394.

Kasten, S., Glasby, G., Schulz, H., Friedrich, G., Andreev, S., 1998. Rare earth elements in manganese nodules from the South Atlantic Ocean as indicators of oceanic bottom water flow. Mar. Geol. 146, 33–52.

Kim, J., Hyeong, K., Lee, H.-B., Ko, Y.-T., 2012. Relationship between polymetallic nodule genesis and sediment distribution in the KODOS (Korea Deep Ocean Study) Area, Northeastern Pacific. Ocean Sci. 47, 197–207.

Klitgord, K.D., Mammerickx, J., 1982. Northern East Pacific Rise: magnetic anomaly and

bathymetric framework. J. Geophys. Res. Solid Earth 87, 6725–6750.

Koppers, A.A.P., Watts, A.B., 2010. Intraplate seamounts as a window into deep earth processes. Oceanography 23, 42–57.

Koppers, A.A.P., Staudigel, H., Pringle, M.S., Wijbrans, J.R., 2003. Short-lived and discontinuous intraplate volcanism in the South Pacific: hot spots or extensional volcanism? Geochem. Geophys. Geosyst. 4. http://dx.doi.org/10.1029/2003GC000533.

Kotlinski, R., Stoyanova, V., Tkatchenko, G., 1996. Environmental studies on a reference transect in the IOM Pioneer Area. In: 6th International Offshore and Polar Engineering Conference. International Society of Offshore and Polar Engineers, Los Angeles, pp. 54–57.

Kotlinski, R., Yubko, V., Stoyanova, V., 2009. Effects of the structural-tectonic and volcanic processes on formation of polymetallic nodules in the CCZ. In: 15th ISA Geological Workshop, Kingston, Jamaica.

Llave, E., Hernández-Molina, F.J., Somoza, L., Stow, D.A.V., Diaz Del Rio, V., 2007. Quaternary evolution of the contourite depositional system in the Gulf of Cadiz. In: Viana, A.R., Rebesco, M. (Eds.), Economic and Palaeoceanographic Significance of Contourite Deposits. Geological Society, London, Special Publications, pp. 49–79.

Lonsdale, P., 1981. Drifts and ponds of reworked pelagic sediment in part of the Southwest Pacific. Mar. Geol. 43, 153–193.

Lonsdale, P., Spiess, F., 1977. Abyssal bedforms explored with a deeply towed instrument package. Mar. Geol. 23, 57–75.

Macdonald, K.C., 1998. Linkages between faulting, volcanism, hydrothermal activity and segmentation on fast spreading centers. In: Faulting and Magmatism at Mid-ocean Ridges, pp. 27–58.

Macdonald, K.C., Sempere, J.-C., Fox, P.J., 1984. East Pacific Rise from Siqueiros to Orozco Fracture Zones: along-strike continuity of axial neovolcanic zone and structure and evolution of overlapping spreading centers. J. Geophys. Res. Solid Earth 89, 6049–6069.

Macdonald, K.C., Sempere, J.-C., Fox, P.J., 1986. Reply: The debate concerning overlapping spreading centers and Mid-Ocean Ridge processes. J. Geophys. Res. 91, 10501–10511.

Macdonald, K.C., Fox, P.J., Alexander, R.T., Pockalny, R., Gente, P., 1996. Volcanic growth faults and the origin of Pacific abyssal hills. Nature 380, 125–129.

Macdonald, A.M., Mecking, S., Robbins, P.E., Toole, J.M., Johnson, G.C., Talley, L., Cook, M., Wijffels, S.E., 2009. The WOCE-era 3-D Pacific Ocean circulation and heat budget. Prog. Oceanogr. 82, 281–325.

Mangini, A., Dominik, J., Müller, P.J., Stoffers, P., 1982. Pacific deep circulation: a velocity increase at the end of the interglacial stage 5? Deep Sea Res. Part A 29, 1517–1530.

Mantyla, A.W., Reid, J.L., 1983. Abyssal characteristics of World's Ocean waters. Deep-Sea Res. 30, 805–833.

Marcantonio, F., Anderson, R.F., Higgins, S., Stute, M., Schlosser, P., Kubik, P., 2001. Sediment focusing in the central equatorial Pacific Ocean. Paleoceanography 16, 260–267.

Margolis, S.V., Burns, R.G., 1976. Pacific deep-sea manganese nodules: their distribution, composition and origin. Annu. Rev. Earth Planet. Sci. 4, 229–263.

McCave, I.N., Carter, L., 1997. Recent sedimentation beneath the Deep Western Boundary Current off northern New Zealand. Deep-Sea Res. I Oceanogr. Res. Pap. 44, 1203–1237.

Menard, H.W., 1959. Geology of the pacific sea floor. Experientia 15, 205–213.

Menard, H.W., 1964. Marine Geology of the Pacific. McGraw-Hill, New York.

Menard, H.W., 1978. Fragmentation of the Farallon plate by pivoting subduction. J. Geol. 86, 99–110.

Mewes, K., Mogollón, J.M., Picard, A., Rühlemann, C., Kuhn, T., Nöthen, K., Kasten, S., 2014. Impact of depositional and biogeochemical processes on small scale variations in nodule abundance in the Clarion-Clipperton Fracture Zone. Deep-Sea Res. I Oceanogr. Res. Pap. 91, 125–141.

Mewes, K., Mogollón, J.M., Picard, A., Rühlemann, C., Eisenhauer, A., Kuhn, T., Ziebis, W., Kasten, S., 2016. Diffusive transfer of oxygen from seamount basaltic crust into overlying sediments: an example from the Clarion–Clipperton Fracture Zone. Earth Planet. Sci. Lett. 433, 215–225.

Michels, K.H., Kuhn, G., Hillenbrand, C.D., Diekmann, B., Futterer, D.K., Grobe, H., Uenzelmann-Neben, G., 2002. The southern Weddell Sea: combined contourite-turbidite sedimentation at the southeastern margin of the Weddell Gyre. In: Stow, D.A.V., Pudsey, C.J., Howe, J.A., Faugères, J.-C., Viana, A.R. (Eds.), Deep-water Contourite Systems: Modern Drifts and Ancient Series, Seismic and Sedimentary Characteristics. Geological Society, London, Memoirs, pp. 305–323.

Mitchell, N.C., Lyle, M.W., Knappenberger, M.B., Liberty, L.M., 2003. Lower Miocene to present stratigraphy of the equatorial Pacific sediment bulge and carbonate dissolution anomalies. Paleoceanography 18, 1038.

Morgan, C.L., Odunton, N.A., Jones, A.T., 1999. Synthesis of environmental impacts of deep seabed mining. Mar. Georesour. Geotechnol. 17, 307–356.

Mulder, T., Voisset, M., Lecroart, P., Le Drezen, E., Gonthier, E., Hanquiez, V., Faugères, J.-C., Habgood, E., Hernández-Molina, F., Estrada, F., 2003. The Gulf of Cadiz: an unstable giant contouritic levee. Geo-Mar. Lett. 23, 7–18.

Mulder, T., Faugères, J.C., Gonthier, E., 2008. Mixed turbidite–contourite systems. In: Rebesco, M., Camerlenghi, A. (Eds.), Contourites, Developments in Sedimentology. 60. Elsevier, pp. 435–456.

Müller, R.D., Sdrolias, M., Gaina, C., Roest, W.R., 2008. Age, spreading rates, and spreading asymmetry of the world's ocean crust. Geochem. Geophys. Geosyst. 9. http://dx.doi.org/10.1029/2007GC001743.

Nishimura, A., 1992. Sedimentation and hiatuses in the central Pacific Basin: their relationship to manganese nodule formation. In: Keating, B.H., Bolton, B.R. (Eds.), Geology and Offshore Mineral Resources of the Central Pacific Basin. Springer, New York, pp. 179–203.

Palomino, D., Vázquez, J.-T., Ercilla, G., Alonso, B., López-González, N., Díaz-del-Río, V., 2011. Interaction between seabed morphology and water masses around the seamounts on the Motril Marginal Plateau (Alboran Sea, Western Mediterranean). Geo-Mar. Lett. 31, 465–479.

Pautot, G., Melguen, M., 1975. Deep Bottom Currents, Sedimentary Hiatuses and

Polymetallic Nodules. International Workshop on Geology, Mineral Resources, and Geophysics of the South Pacific (IDOE Workshop), Suva, Fiji, pp. 227–234.

Pautot, G., Melguen, M., 1979. Influence of deep water circulation and sea floor morphology on the abundance and grade of central south Pacific manganese nodules. In: Bischoff, J.L., Piper, D.Z. (Eds.), Marine Geology and Oceanography of the Pacific Manganese Nodule Province. Springer US, pp. 621–649.

Polzin, K., Toole, J., Ledwell, J., Schmitt, R., 1997. Spatial variability of turbulent mixing in the abyssal ocean. Science 276, 93–96.

Price, N.B., Calvert, S.E., 1970. Compositional variation in Pacific Ocean ferromanganese nodules and its relationship to sediment accumulation rates. Mar. Geol. 9, 145–171.

Rebesco, M., Camerlenghi, A., 2008. Contourites. In: Developments in Sedimentology 60. Elsevier, Amsterdam.

Rebesco, M., Camerlenghi, A., Volpi, V., Neagu, C., Accettella, D., Lindberg, B., Cova, A., Zgur, F., 2007. Interaction of processes and importance of contourites: insights from the detailed morphology of sediment Drift 7, Antarctica. In: Viana, A.R., Rebesco, M. (Eds.), Economic and Palaeoceanographic Significance of Contourite Deposits. Geological Society, London, Special Publications, pp. 95–110.

Rebesco, M., Hernández-Molina, F.J., Van Rooij, D., Wåhlin, A., 2014. Contourites and associated sediments controlled by deep-water circulation processes: state-of-the-art and future considerations. Mar. Geol. 352, 111–154.

Reid, J.L., 1986. On the total geostrophic circulation of the South Pacific Ocean: flow patterns, tracers and transports. Prog. Oceanogr. 16, 1–61.

Rintoul, S.R., 2013. Large-scale ocean circulation: deep circulation and meridional overturning. In: Orcutt, J. (Ed.), Earth System Monitoring: Selected Entries From the Encyclopedia of Sustainability Science and Technology. Springer New York, New York, NY, pp. 199–232.

Roden, G.I., 1987. Effect of seamounts and seamount chains on ocean circulation and thermohaline structure. In: Seamounts, Islands, and Atolls 43, pp. 335–354.

Ruellan, E., Huchon, P., Auzende, J.-M., Gracia, E., 1994. Propagating rift and overlapping spreading center in the North Fiji Basin. Mar. Geol. 116, 37–56.

Rühlemann, C., Kuhn, T., Wiedicke, M., Kasten, S., Mewes, K., Picard, A., 2011. Current status of manganese nodule exploration in the German license area. In: 9th ISOPE Ocean Mining Symposium. International Society of Offshore and Polar Engineers, Maui, Hawaii, pp. 168–173.

Schmidt, R., Schmincke, H.-U., 2000. Seamounts and island building. In: Encyclopedia of Volcanoes, pp. 383–402.

Sempere, J.-C., Macdonald, K.C., Miller, S.P., 1984. Overlapping spreading centres: 3-D inversion of the magnetic field at 9°03′ on the East Pacific Rise. Geophys. J. Int. 79, 799–811.

Shanmugam, G., 2008. Deep-water bottom currents and their deposits. In: Rebesco, M., Camerlenghi, A. (Eds.), Contourites, Developments in Sedimentology 60. Elsevier, pp. 59–81.

Shanmugam, G., 2013. Modern internal waves and internal tides along oceanic pycnoclines: challenges and implications for ancient deep-marine baroclinic sands. AAPG Bull. 97, 799–843.

Shanmugam, G., 2014. Modern internal waves and internal tides along oceanic pycnoclines: challenges and implications for ancient deep-marine baroclinic sands: reply. AAPG Bull. 98, 858–879.

Shipley, T.H., Winterer, E.L., Goud, M., Mills, S.J., Metzler, C.V., Paull, C.K., Shay, J.T., 1985. Seabeam bathymetric and water-gun seismic reflection surveys in the equatorial Pacific. Initial Rep. Deep Sea Drill. Proj. 85, 825–837.

Shor, G.G., 1958. Reflexion studies in the eastern equatorial Pacific. Deep-Sea Res. 5, 283–289.

Skornyakova, N.S., Murdmaa, I.O., 1992. Local variations in distribution and composition of ferromanganese nodules in the Clarion-Clipperton Nodule Province. Mar. Geol. 103, 381–405.

Sloan, H., 1991. Temporal evolution of overlapping spreading centers at 16°20′N on the East Pacific Rise. Mar. Geol. 97, 315–324.

Smith, A.D., 2007. A plate model for Jurassic to recent intraplate volcanism in the Pacific Ocean basin. Geol. Soc. Am. Spec. Pap. 430, 471–495.

Smith, D.K., Jordan, T.H., 1988. Seamount statistics in the Pacific Ocean. J. Geophys. Res. Solid Earth 93, 2899–2918.

Smoot, N.C., Choi, D.R., 2003. The North Pacific megatrend. Int. Geol. Rev. 45, 346–370.

St Laurent, L.C., Garrett, C., 2002. The role of internal tides in mixing the deep ocean. J. Phys. Oceanogr. 32, 2882–2899.

Staudigel, H., Clague, D.D., 2010. The geological history of deep-sea volcanoes: biosphere, hydrosphere and litosphere interactions. Oceanography 23, 58–71.

Stow, D.A.V., Pudsey, C.J., Howe, J.A., Faugères, J.C., Viana, A.R., 2002a. Deep-water Contourite Systems. Modern Drifts and Ancient Series, Seismic and Sedimentary Characteristics. Geological Society of London Memoirs, pp. 22.

Stow, D.A.V., Faugères, J.C., Howe, J.A., Pudsey, C.J., Viana, A.R., 2002b. Bottom currents, contourites and deep-sea sediment drifts: current state-of-the-art. In: Stow, D.A.V., Pudsey, C.J., Howe, J.A., Faugères, J.-C., Viana, A.R. (Eds.), Deep-water Contourite Systems: Modern Drifts and Ancient Series, Seismic and Sedimentary Characteristics. Geological Society, London, Memoirs, pp. 7–20.

Stow, D.A.V., Faugères, J.C., Gonthier, E., Cremer, M., Llave, E., Hernández-Molina, F.J., Somoza, L., Diaz-Del-Rio, V., 2002c. Faro-Albufeira drift complex, northern Gulf of Cadiz. In: Stow, D.A.V., Pudsey, C.J., Howe, J.A., Faugères, J.-C., Viana, A.R. (Eds.), Deep-water Contourite Systems: Modern Drifts and Ancient Series, Seismic and Sedimentary Characteristics. Geological Society, London, Memoirs, pp. 137–154.

Stow, D.A.V., Hernández-Molina, F.J., Llave, E., Sayago-Gil, M., Diaz del Rio, V., Branson, A., 2009. Bedform-velocity matrix: the estimation of bottom current velocity from bedform observations. Geology 37, 327–330.

Talley, L.D., Joyce, T.M., 1992. The double silica maximum in the North Pacific. J. Geophys. Res. 97, 5465–5480.

Tracey, J., Sutton, G., Nesteroff, W., Galehouse, J., von der Borch, C., Moore, T., Lipps, J., Haq, B.U., Beckmann, J., 1971. Initial Reports of the Deep Sea Drilling Project. US Government Printing Office, Washington.

Tsuchiya, M., Talley, L.D., 1996. Water-property distributions along an eastern Pacific hydrographic section at 135°W. J. Mar. Res. 54, 541–564.

Tucholke, B.E., 2002. The Greater Antilles Outer Ridge: development of a distal sedimentary drift by deposition of fine-grained contourites. In: Stow, D.A.V., Pudsey, C.J., Howe, J.A., Faugères, J.-C., Viana, A.R. (Eds.), Deep-water Contourite Systems: Modern Drifts and Ancient Series, Seismic and Sedimentary Characteristics. Geological Society, London, Memoirs, pp. 39–55.

Van Andel, T.H., Heath, G.R., Moore, T.C., 1975. Cenozoic history and paleoceanography of the central equatorial Pacific ocean: a regional synthesis of Deep Sea Drilling Project data. Geol. Soc. Am. Mem. 143, 1–223.

Van Rooij, D., Blamart, D., Kozachenko, M., Henriet, J.P., 2007. Small mounded contourite drifts associated with deep-water coral banks, Porcupine Seabight, NE Atlantic Ocean. In: Viana, A.R., Rebesco, M. (Eds.), Economic and Palaeoceanographic Significance of Contourite Deposits. Geological Society, London, Special Publications, pp. 225–244.

Van Rooij, D., Iglesias, J., Hernández-Molina, F., Ercilla, G., Gomez-Ballesteros, M., Casas, D., Llave, E., De Hauwere, A., Garcia-Gil, S., Acosta, J., 2010. The Le Danois Contourite depositional system: interactions between the Mediterranean outflow water and the upper Cantabrian slope (North Iberian margin). Mar. Geol. 274, 1–20.

Van Rooij, D., Campbell, C., Rueggeberg, A., Wahlin, A., 2016. The contourite log-book: significance for palaeoceanography, ecosystems and slope instability. In: Marine Geology Special Issue. Elsevier.

Vandorpe, T., Van Rooij, D., de Haas, H., 2014. Stratigraphy and paleoceanography of a topography-controlled contourite drift in the Pen Duick area, southern Gulf of Cádiz. Mar. Geol. 349, 136–151.

Vandorpe, T., Martins, I., Vitorino, J., Hebbeln, D., García, M., Van Rooij, D., 2016. Bottom currents and their influence on the sedimentation pattern in the El Arraiche mud volcano province, southern Gulf of Cadiz. Mar. Geol. 378, 114–126.

Verfaillie, E., Doornenbal, P., Mitchell, A., White, J., Van Lancker, V., 2007. The bathymetric position index (BPI) as a support tool for habitat mapping. In: Worked Example for the MESH Final Guidance, pp. 1–14.

Viana, A.R., Rebesco, M., 2007. Economic and palaeoceanographic significance of contourite deposits. Geol. Soc. Spec. Publ. 276.

von Stackelberg, U., Beiersdorf, H., Riech, Volkher, 1987. Relationship between manganese nodule formation and sedimentary processes in the equatorial north Pacific ocean: a synthesis based on the results of Cruise SO 25 (1982) with RV Sonne. In: von Stackelberg, U., Beiersdorf, H. (Eds.), Manganese Nodules and Sediments in the Equatorial North Pacific Ocean. Geologisches Jahrbuch Reiche D 87, pp. 377–403.

von Stackelberg, U., Beiersdorf, H., 1991. The formation of manganese nodules between the Clarion and Clipperton fracture zones southeast of Hawaii. Mar. Geol. 98, 411–423.

Weiss, A., 2001. Topographic Position and Landforms Analysis (Poster presentation). ESRI User Conference, San Diego, CA, pp. 200.

Wessel, P., Sandwell, D.T., Kim, S.-S., 2010. The global seamount census. Oceanography 23, 24–33.

White, S.M., Mason, J.L., Macdonald, K.C., Perfit, M.R., Wanless, V.D., Klein, E.M., 2009. Significance of widespread low effusion rate eruptions over the past two million years for delivery of magma to the overlapping spreading centers at 9°N East Pacific Rise. Earth Planet. Sci. Lett. 280, 175–184.

Whittaker, J.M., Goncharov, A., Williams, S.E., Müller, R.D., Leitchenkov, G., 2013. Global sediment thickness data set updated for the Australian-Antarctic Southern Ocean. Geochem. Geophys. Geosyst. 14, 3297–3305.

Wijffels, S.E., Toole, J.M., Bryden, H.L., Fine, R.A., Jenkins, W.J., Bullister, J.L., 1996. The water masses and circulation at 10°N in the Pacific. Deep-Sea Res. I 43, 501–544.

Wright, I.C., Graham, I.J., Chang, S.W., Choi, H., Lee, S.R., 2005. Occurrence and physical setting of ferromanganese nodules beneath the Deep Western Boundary Current, Southwest Pacific Ocean. N. Z. J. Geol. Geophys. 48, 27–41.

Wright, D.J., Pendleton, M., Boulware, J., Walbridge, S., Gerlt, B., Eslinger, D., Sampson, D., Huntley, E., 2012. ArcGIS Benthic Terrain Modeler (BTM), v. 3.0. Environmental Systems Research Institute, NOAA Coastal Services Center, Massachusetts Office of Coastal Zone Management.

Yubko, V.M., 2016. Model of CCZ geological-geomorphological structure and nodules potential formation. In: Minerals of the Ocean VIII & Deep-sea Minerals and Mining V, St.Petersburg, Russia, pp. 213–216.

Zenk, W., 2001. Abyssal currents in the world's ocean. In: Steele, J.H., Thope, S.A., Turekian, K.K. (Eds.), Encyclopedia of Ocean Science. Academic Press, London, pp. 12–28.

Zenk, W., 2008. Abyssal and contour currents. In: Rebesco, M., Camerlenghi, A. (Eds.), Contourites, Developments in Sedimentology. 60. Elsevier, pp. 35–57.

Zhang, L., Buijsman, M.C., Comino, E., Swinney, H.L., 2017. Internal wave generation by tidal flow over periodically and randomly distributed seamounts. J. Geophys. Res. Oceans 122, 5063–5074.